Interactions of plutons and detachments, comparison of Aegean and Tyrrhenian granitoids

Laurent Jolivet, Laurent Arbaret, Laetitia Le Pourhiet, Florent Cheval-Garabedian, Vincent Roche, Aurélien Rabillard, Loïc Labrousse

https://doi.org/10.5194/se-2021-11
Preprint. Discussion started: 16 February 2021

Solid Earth
Discussions
Open Access
EGU

Interactions of plutons and detachments, comparison of Aegean and Tyrrhenian granitoids

Laurent Jolivet [1], Laurent Arbaret [2,3,4], Laetitia Le Pourhiet [1], Florent Cheval-Garabedian [2,3,4], Vincent Roche [1], Aurélien Rabillard [2,3,4], Loïc Labrousse [1]

[1] Sorbonne Université, CNRS-INSU, Institut des Sciences de la Terre Paris, ISTeP UMR 7193, F-75005 Paris, France
[2] Université d'Orléans, ISTO, UMR 7327, 45071, Orléans, France
[3] CNRS/INSU, ISTO, UMR 7327, 45071 Orléans, France
[4] BRGM, ISTO, UMR 7327, BP 36009, 45060 Orléans, France

Abstract: Back-arc extension superimposed on mountain belts leads to distributed normal faults and shear zones, interacting with magma emplacement in the crust. The composition of granitic magmas emplaced at this stage often involves a component of crustal melting. The Miocene Aegean granitoids were emplaced in metamorphic core complexes (MCC) below crustal-scale low-angle extensional shear zones and normal faults. Intrusion in such contexts interacts with extension and shear along detachments, from the hot magmatic flow within the pluton root zone to the colder ductile and brittle deformation along the detachment. A comparison of the Aegean plutons with the Elba Island MCC in the back-arc region of the Apennines subduction shows that these processes are characteristic of pluton-detachment interactions in general and we discuss a conceptual emplacement scenario, tested by numerical models. Mafic injections within the partially molten lower crust above the hot asthenosphere trigger the ascent within the core of the MCC of felsic magmas, controlled by the strain localization on persistent crustal scale shear zones at the top that guide the ascent until the brittle ductile transition is reached during exhumation. Once the system definitely enters the brittle regime, the detachment and the upper crust are intruded while new detachments migrate upward and in the direction of shearing. Numerical models reproduce the geometry and the kinematic evolution deduced from field observations.

https://doi.org/10.5194/se-2021-11
Preprint. Discussion started: 16 February 2021

1. Introduction

In the deep parts of orogens, the flow of melts is coupled with ductile deformation and controlled by buoyancy and tectonic forces (Brown, 1994; Brown and Solar, 1998; Brown, 2007). Migmatites, which are weak crustal material as long as they are kept at high temperature, are the source of magmas that concentrate within plutons of various sizes. On the other hand, interactions between magmatism and lithospheric deformation, and more specifically interactions of plutons with crustal-scale tectonics, depend first of all upon the rate of magma production and, to a second order, strain rates. The rate of magma transfer to the crust is indeed so large compared to tectonic strain rates that the construction of plutons is thought in a first approach to be little influenced by the tectonic setting, especially when small plutons are concerned (de Saint Blanquat et al., 2011).

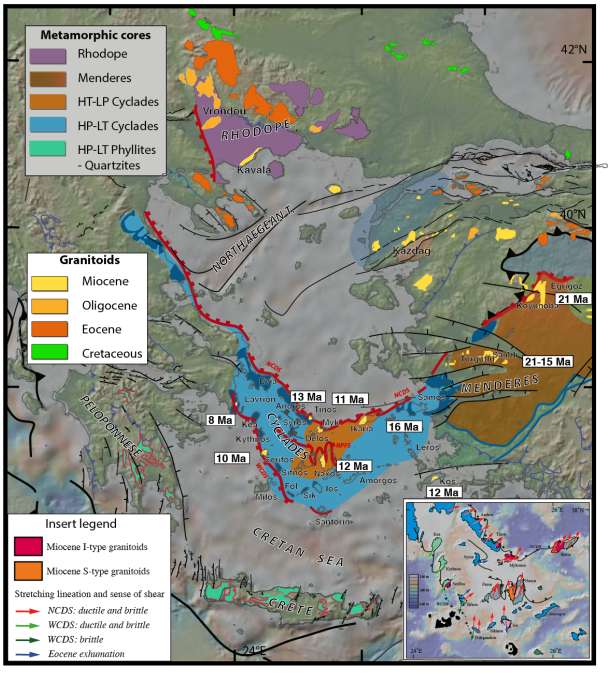

Figure 1: Tectonic map of the Aegean region showing the successive generations of granitoids since the late Cretaceous. Modified from Jolivet et al. (2015).

The Miocene Aegean plutons (figure 1), emplaced in an extensional context within metamorphic core complexes (MCCs), may however depart from this behaviour. Despite a moderate volume, they have indeed recorded the complete evolution from syn-tectonic magmatic flow to localized mylonitic deformation along the main detachment (Faure and Bonneau, 1988; Urai et al., 1990; Faure et al., 1991; Lee and Lister, 1992; Gautier et al., 1993;

https://doi.org/10.5194/se-2021-11
Preprint. Discussion started: 16 February 2021

Solid Earth
Discussions
Open Access
EGU

Laurent et al., 2015; Rabillard et al., 2015; Bessière et al., 2017; Rabillard et al., 2018). All of them moreover show a systematic magmatic and tectonic evolution of the host MCCs with several magmatic pulses and a series of detachments forming sequentially during exhumation (Rabillard et al., 2018). Several of them also show an association of mixed or mingled felsic and mafic magmas, with an evolution from a significant component of crustal melting toward more mafic composition, a trend that is common in post-orogenic magmas (Bonin, 2004).

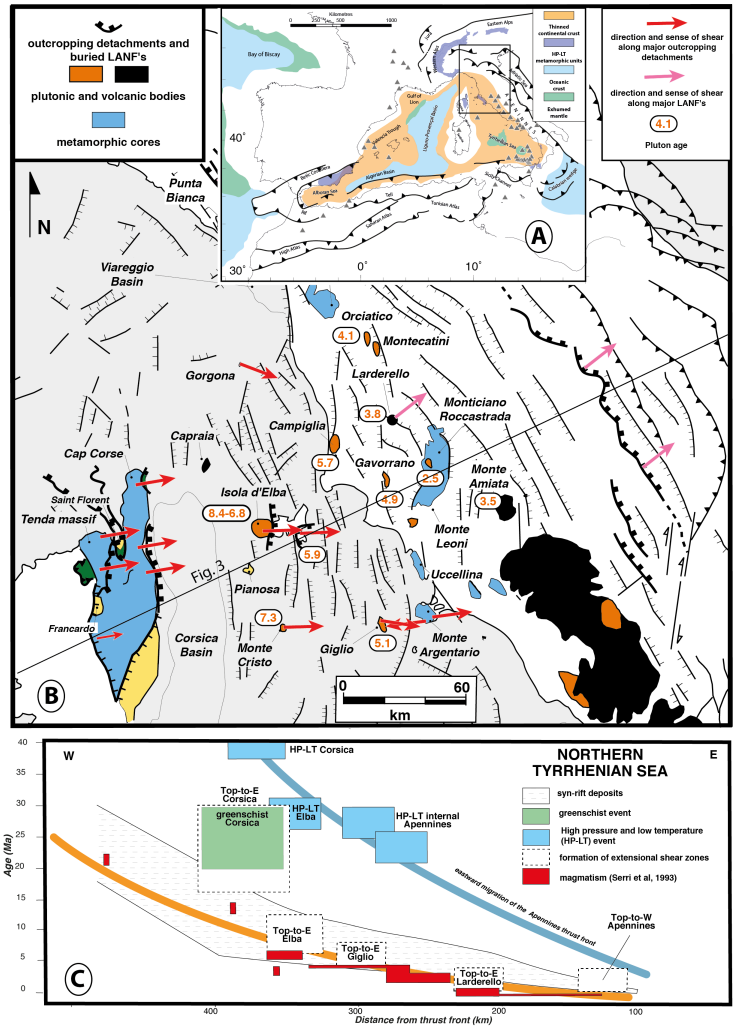

Figure 2: Tectonic map of the Central and Western Mediterranean with the distribution of recent magmatism (Savelli, 1988; Serri et al., 1993; Savelli, 2002b, a; Duggen et al., 2005; Avanzinelli et al., 2009; Savelli, 2015). Tectonic map (B) of the northern Tyrrhenian region and Northern Apennines and (C) a diagram showing the evolution of the ages of syn-rift basins, metamorphic events and magmatism along a cross-section from Corsica to the Apennines, modified from Jolivet et al. (1998).

https://doi.org/10.5194/se-2021-11
Preprint. Discussion started: 16 February 2021

Solid Earth
Discussions
Open Access
EGU

Whether these features are characteristic of syn-extension plutons in post-orogenic back-arc environments is the question we address in this paper, through a comparison of the Aegean plutons with those of the northern Tyrrhenian Sea and Tuscany, with a focus on Elba Island in the Tuscan archipelago (figure 2). Striking similarities can indeed be observed between the two contexts in terms of tectonic and magmatic evolution. We propose and test a scenario of formation and emplacement of plutons in a back-arc post-orogenic context below crustal-scale detachments.

2. Geodynamic context

The Aegean and North Tyrrhenian granitoids were emplaced during the Miocene and part of the early Pliocene in the back-arc regions of the Hellenic and Apennines subduction, respectively (Serri et al., 1993; Jolivet et al., 1998; Pe-Piper and Piper, 2002, 2007; Avanzinelli et al., 2009; Jolivet et al., 2015; Rabillard et al., 2018) (figure 3).

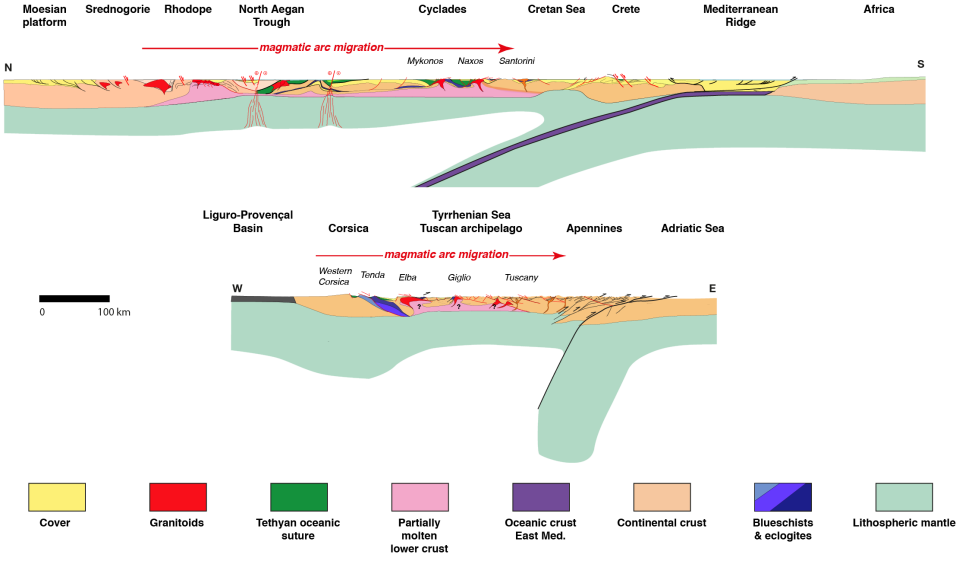

Figure 3: Two lithospheric-scale cross-sections of the Aegean domain (Jolivet and Brun, 2010) and the Northern Tyrrhenian Sea and the Apennines (Jolivet et al., 1998).

These two subduction zones started to retreat approximately at the same time, 30-35 Ma ago (Jolivet and Faccenna, 2000). A first-order change in the geodynamics of this region indeed occurred at this period, also coeval with the hard collision between Africa and Eurasia in the eastern and westernmost Mediterranean. The subducting African lithosphere, locked between two collision zones, continued to subduct northward but with a significant component of retreat.

https://doi.org/10.5194/se-2021-11
Preprint. Discussion started: 16 February 2021

Since that time subduction has been continuous, with however several episodes of slab detachment and tearing (Wortel and Spakman, 2000; Spakman and Wortel, 2004; Faccenna and Becker, 2010; Faccenna et al., 2014). The Aegean plutons studied in this paper were emplaced during the formation of a large tear in the subducting lithosphere between 16 and 8 Ma (Jolivet et al., 2015). The oldest North Tyrrhenian pluton is dated around 7 Ma in Elba (Westerman et al., 2004) and the youngest ones, Pliocene in age (Serri et al., 1993), are currently exploited for geothermal energy in Tuscany (Rossetti et al., 2008; Rochira et al., 2018). All these plutons contain a significant component of crustal melts and some of them are linked with migmatite domes such as on Naxos, Mykonos and Ikaria (Jansen, 1977; Urai et al., 1990; Denèle et al., 2011; Beaudoin et al., 2015; Vanderhaeghe et al., 2018). Mixing and mingling with mafic magmas are also observed in some of these plutons and the general evolution shows an increase of the mantle component with time.

Most of these plutons are associated with low-angle normal faults (LANF) and shear zones and they were emplaced in the core of MCCs (Faure et al., 1991; Lee and Lister, 1992; Lister and Baldwin, 1993; Daniel and Jolivet, 1995; Jolivet et al., 1998; Berger et al., 2013; Bessière et al., 2017; Rabillard et al., 2018). These LANF and associated ductile shear zones (we use the term "detachment" for the whole structure, brittle and ductile) started to form before the emplacement of the plutons, in both regions. The main difference between the two regions are the kinematics of these detachments (figure 3) (Jolivet et al., 2008) and the role of tectonic inheritance. In the Aegean, most of the MCCs are capped by north-dipping detachments except in the southwest where south-dipping detachments are observed. The north-dipping detachments probably partly reactivate former thrusts related to the building of the Hellenides orogenic wedge. In the Northern Tyrrhenian Sea and in Tuscany, all detachments dip eastward, i.e. toward the subduction zone. In that case, the detachments cannot reactivate the former thrusts of the internal Apennines that dip westward. Only in the case of the oldest detachments, found in Alpine Corsica, can they correspond to reactivated thrusts. The case of Elba Island shows the detachments cutting down-section eastward within the stack of former nappes (Keller and Pialli, 1990; Collettini and Holdsworth, 2004). Whatever the nature (i.e. reactivated structure or not) and the sense of shear of these detachments, the interaction with the plutons follows a similar pattern that we recall below, first briefly for the Aegean region and then for Elba Island (see Rabillard et al., 2018, for details on the Aegean).

https://doi.org/10.5194/se-2021-11
Preprint. Discussion started: 16 February 2021

3. Aegean plutons

The Miocene Aegean and Menderes plutons were emplaced during a short time period between ~20 Ma and 8 Ma, the oldest cropping out in the Menderes massif and the youngest in the western part of the Aegean region (figures 1, 3) (Jolivet et al., 2015). Those occupying the Cycladic domain are all associated with detachments, either north or south-dipping (figure 4) (Grasemann and Petrakakis, 2007; Rabillard et al., 2018).

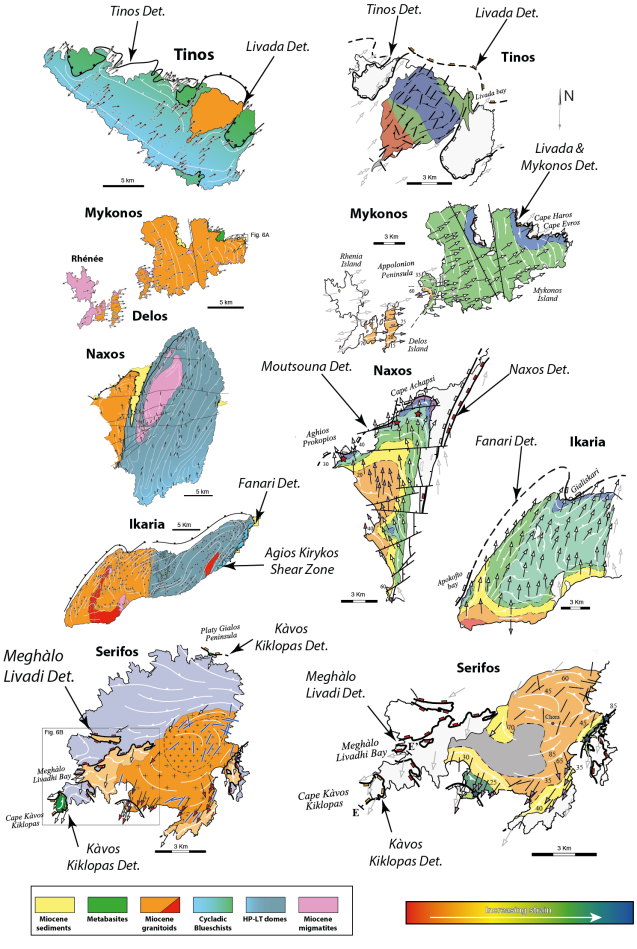

Figure 4: Five examples of the Aegean granitoids showing the interactions between deformation and intrusion, after Rabillard et al. (2018) and references therein. The left column show maps of the entire islands and the right column shows the internal fabrics of the plutons. These maps were obtained based on deformation grades observed in the field, a scale of grades was designed for each pluton to describe the gradients. Arrows show stretching lineations and sense of shear and black bars on the Tinos and Serifos plutons shows the direction of the magnetic lineation.

https://doi.org/10.5194/se-2021-11
Preprint. Discussion started: 16 February 2021

136

137 Except for Serifos and Lavrion plutons, associated with the West Cycladic Detachment
138 System (WCDS) (Grasemann and Petrakakis, 2007; Berger et al., 2013; Scheffer et al., 2016),
139 the plutons crop out in the core of MCCs exhumed by north-dipping detachments, such as the
140 North Cycladic Detachment System (NCDS) (Gautier and Brun, 1994b, a; Jolivet et al., 2010)
141 or the Naxos-Paros Fault System (NPFS) (Urai et al., 1990; Gautier et al., 1993; Vanderhaeghe,
142 2004; Bargnesi et al., 2013; Cao et al., 2017). The detachments upper plate is made of the Upper
143 Cycladic Nappe, a remnant of the Pelagonian domain, made of greenschists-facies metabasites
144 or serpentinite with, in a few cases, early to late Miocene sediments deposited during extension
145 (Angelier et al., 1978; Sanchez-Gomez et al., 2002; Kuhlemann et al., 2004; Menant et al.,
146 2013). The MCCs are made of various units of the Cycladic Blueschists, more or less
147 retrograded in the greenschist-facies, or the Cycladic basement, showing H*T*-L*P* metamorphic
148 facies and even anatectic conditions on several islands, such as Naxos, Paros, Mykonos or Ikaria
149 (Buick and Holland, 1989; Urai et al., 1990; Buick, 1991; Keay et al., 2001; Duchêne et al.,
150 2006; Seward et al., 2009; Kruckenberg et al., 2011; Beaudoin et al., 2015; Laurent et al., 2015;
151 Rabillard et al., 2015; 2018). The plutons intruded these MCCs and were sheared at the top by
152 the detachments during their emplacement (Rabillard et al., 2018).
153 The granitoids show a variety of facies and composition, but most of them have a crustal
154 melting component and some are closely associated with migmatites, as on Ikaria or Mykonos
155 (Vanderhaeghe, 2009; Kruckenberg et al., 2011; Denèle et al., 2011; Beaudoin et al., 2015;
156 Jolivet et al., 2021). Compositions show a common trend for these plutons indicating that they
157 crystallized primarily from I-type magmas with some contamination by the continental crust
158 and little fractionation (figure A1, Appendix A). Field evidence show a close association of
159 these I-type intrusions with two-micas granites (in Ikaria for instance), migmatites, or both
160 (Ikaria, Naxos, Paros, Rheneia-Delos) (Pe-Piper et al., 1997; Pe-Piper, 2000; Pe-Piper et al.,
161 2002; Vanderhaeghe, 2004; Bolhar et al., 2010; Bolhar et al., 2012; Bargnesi et al., 2013;
162 Beaudoin et al., 2015; Laurent et al., 2015; Jolivet et al., 2021). Tinos, Ikaria and Serifos
163 granitoids were emplaced in several magma batches with an evolution through time,
164 characterized by more and more mafic compositions and a decrease of the grain size
165 (Grasemann and Petrakakis, 2007; Ring, 2007; Bolhar et al., 2010; Petrakakis et al., 2010;
166 de Saint Blanquat et al., 2011; Bolhar et al., 2012; Beaudoin et al., 2015; Laurent et al., 2015;
167 Rabillard et al., 2015; Ducoux et al., 2016). On Serifos and Naxos, the farthest parts of the
168 pluton from the detachment show an enrichment in mafic enclaves and evidence for magma

https://doi.org/10.5194/se-2021-11
Preprint. Discussion started: 16 February 2021

169 mixing and mingling in the roots of the rising plutons (Rabillard et al., 2015; Bessière et al.,
170 2017; Rabillard et al., 2018).

171 A common evolution is observed in several of these plutons during their interaction with
172 the system of detachments exhuming their host MCC (Rabillard et al., 2018). A series of two
173 or three detachments is observed (figure 4, figure 5).

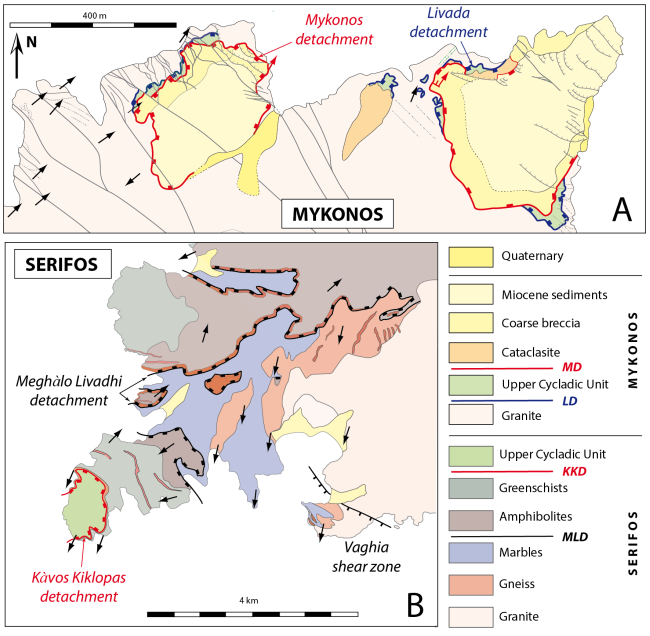

174

175 *Figure 5: Details of the two detachments on Mykonos and Serifos. A: northeastern Mykonos*
176 *(see location on figure 5), B: Southwest Serifos. The Mykonos (MD) and Livada (LD)*
177 *detachments on Mykonos and the mineralized veins and normal faults (baryte and iron-*
178 *hydroxides) – grey- are after Menant et al. (2013). The Kàvos Kiklopas (KKD) and Meghàlo*
179 *Livadi (MLD) detachments on Serifos are after Grasemann and Petrakakis (2007) and*
180 *Ducoux et al. (2016).*
181

182 The deepest one is mostly ductile and has started to act long before the granitic intrusion
183 that ultimately intrudes it. The upper detachments are mostly brittle and are locally intruded by
184 dykes and sills emanating from the main pluton. When a sedimentary basin is present, it is
185 deposited on top of the uppermost detachment during extension and can be partly affected by
186 mineralized veins (Menant et al., 2013). All plutons show a gradient of shearing deformation
187 toward the detachment with an evolution from ductile to brittle (Figure 4). The maps shown in
188 figure 4 were drawn after detailed field observations and the construction of a scale of up to 7
189 grades of progressive deformation, from non-deformed granitic texture to ultra-mylonites, with
190 the progressive appearance of foliation, stretching lineation, localization of C and C' shear

https://doi.org/10.5194/se-2021-11
Preprint. Discussion started: 16 February 2021

bands (Berthé et al., 1979; Lister and Snoke, 1984), for details see Rabillard et al. (2018). The inner parts of the plutons show mixing of acidic and mafic magmas and a co-magmatic deformation, co-axial with the post-solidus deformation along the detachment (Rabillard et al., 2015; 2018). The flow of magma is thus oriented by the regional strain field. Serifos shows (i) a decrease of grain size through time with an inner facies with smaller grain size and finally fine-grained dykes and (ii) evidence for hydrothermalism in the root zone of the pluton, suggesting that the magmatic system was open upward with a possible volcano-plutonic system (Rabillard et al., 2015; 2018).

4. North Tyrrhenian plutons

The Monte Capanne pluton on Elba island (figure 6) is the oldest of a series of plutons cropping out in the Tuscan archipelago and onshore Tuscany (Serri et al., 1993; Westerman et al., 2004; Avanzinelli et al., 2009).

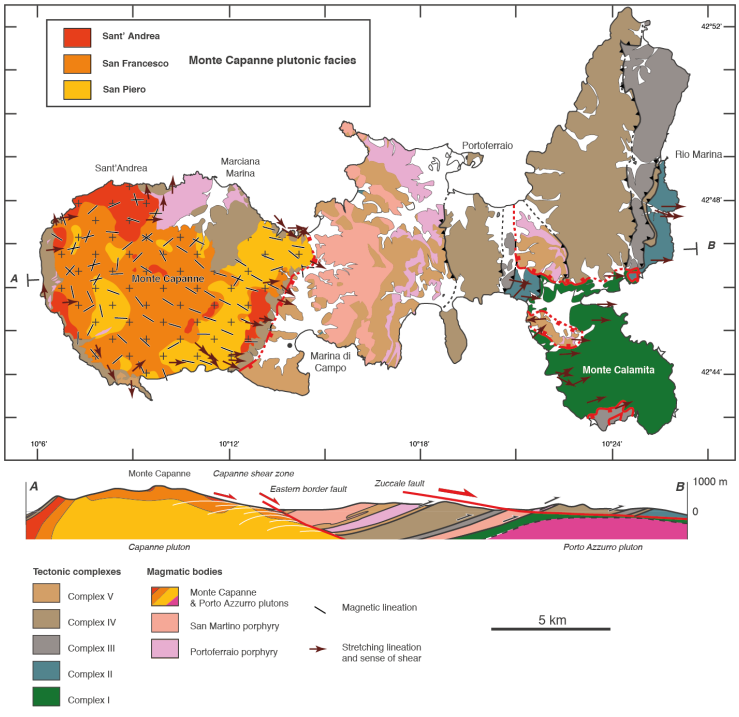

Figure 6: Tectonic map and cross-section of Elba Island showing the main tectonic units and the main extensional shear zones and detachments, modified after Bianco et al. (2015). Details of the internal structure of the Monte Capanne intrusions are reported based on Farina et al. (2010).

https://doi.org/10.5194/se-2021-11
Preprint. Discussion started: 16 February 2021

These plutons belong to magmas migrating from west to east between the end of the Oligocene and the Quaternary, mimicking the migration of the Apennines thrust system and the H*P*-L*T* metamorphism of the internal Apennines and Tuscan Archipelago (Serri et al., 1993; Jolivet et al., 1998) (figure 2). This situation is thus very similar to the Aegean Sea. The decrease of the time lag between the recording of H*P*-L*T* metamorphism or the activation age of the thrust front and the magmatism has been interpreted as a consequence of slab steepening during retreat (Jolivet et al., 1998; Brunet et al., 2000). Pluton ages decrease eastward from ~8 Ma to 2-3 Ma (figure 2). Among the youngest plutons are those powering the active geothermal fields of Larderello and Monte Amiata (Camelli et al., 1993; Brogi et al., 2003; Rossetti et al., 2008). The oldest plutons are observed offshore on Elba (Monte Capanne and Porto Azzuro plutons), Monte Cristo and Giglio islands (Westerman et al., 1993) (figure 2). These four plutons are granodiorites/monzogranites and they all display a contamination with crustal magmas with a main source thought to be lower crustal anatexis (Serri et al., 1993; Innocenti et al., 1997). They were emplaced within an overall extensional context during the rifting of the Northern Tyrrhenian Sea in the back-arc region of the Apennines (Jolivet et al., 1998). First evidenced in Alpine Corsica and on Elba island, a series of east-dipping low-angle detachments controlled the kinematics of extension along the Corsica-Apennines transect from the Oligocene onward (Jolivet et al., 1998). Extension is shown to migrate from west to east with time and it is active at present in the highest altitude regions of the Apennines just west of Corno Grande peak with however west-dipping normal faults (D'Agostino et al., 1998). The youngest east-dipping low-angle normal faults are seismically active in the Alto Tiberina region (Collettini and Barchi, 2002, 2004; Pauselli and Ranalli, 2017). Evidence for top-to-the east shearing deformation is found within the plutons of the Tuscan archipelago, but the detachments crop out nicely mostly on Elba island (Keller and Pialli, 1990; Daniel and Jolivet, 1995; Collettini and Holdsworth, 2004; Liotta et al., 2015).

4.1. Monte Capanne pluton, Elba Island

Elba, the largest island of the Tuscan archipelago, shows the relations between peraluminous magmatic bodies and two east-dipping low-angle shear zones cutting down-section within the Tuscan nappe stack emplaced before extension started (figure 6) (Keller and Pialli, 1990; Bouillin et al., 1993; Pertusati et al., 1993; Daniel and Jolivet, 1995; Westerman et al., 2004; Bianco et al., 2015). Five thrust packages (complexes I to V) are separated by west-dipping low-angle reverse faults (Trevisan, 1950; Barberi et al., 1967; Perrin, 1975; Pertusati

https://doi.org/10.5194/se-2021-11
Preprint. Discussion started: 16 February 2021

et al., 1993; Bianco et al., 2015; Bianco et al., 2019). Long thought free of any H*P*-L*T* imprint, at variance with the nearby Gorgona and Giglio islands where the presence of Fe-Mg-carpholite attest for blueschist-facies metamorphism (Rossetti et al., 1999a; 1999b), the nappe stack has only recently revealed H*P*-L*T* parageneses along the east coast of the island (Bianco et al., 2015). Through a correlation with the H*P*-L*T* units of Gorgona (Rossetti et al., 1999), where $^{40}Ar/^{39}Ar$ dating on micas yielded ages around 25 Ma (Brunet et al., 2000), the Elba blueschists are attributed to the Oligocene-Early Miocene.

The Nappe stack is intruded by the shallow-level San Martino and Portoferraio porphyries coeval with the Monte Capanne pluton (figure 6), spanning a short period between 8 and 6.8 Ma, showing that the magma has intruded the detachment in a late stage (Saupé et al., 1982; Juteau et al., 1984; Ferrara and Tonarini, 1985; Bouillin et al., 1994; Westerman et al., 2004). The Monte Capanne intrusion makes the major part of the western half of the island and the highest peak. It is surrounded by a contact metamorphic aureole developed at the expense of the nappe stack (Duranti et al., 1992; Dini et al., 2002; Rossetti et al., 2007; Rossetti and Tecce, 2008). The metamorphic parageneses within the aureole suggest an emplacement at a depth of 4-5 km (Dini et al., 2002; Rocchi et al., 2002; Farina et al., 2010; Pandeli et al., 2018). The pluton shows an internal deformation with a gradient of shearing toward the east attested by the magnetic fabric, stretching lineation and sense of shear (Bouillin et al., 1993; Daniel and Jolivet, 1995). The pluton and the metamorphic aureole are separated from the nappe stack by an east-dipping low-angle shear zone (Capanne shear zone) evolving into a brittle east-dipping fault (eastern border fault) (Daniel and Jolivet, 1995). Syn-kinematic contact metamorphism minerals coeval with top-to-the east kinematic indicators attest for the syn-kinematic nature of the intrusion (Daniel and Jolivet, 1995; Pandeli et al., 2018).

The eastern part of the island shows granitic dykes emanating from the buried younger Porto Azzuro pluton intruding the Calamiti schists complex (Complex I, figure 6) (Daniel and Jolivet, 1995; Maineri et al., 2003; Musumeci and Vaselli, 2012). Here too, evidence for top-to-the east shearing at the time of intrusion have been described (Daniel and Jolivet, 1995) (figure 7). The pluton and the Calamiti schists are topped by the Zuccale low-angle normal fault that cuts down-section across the entire nappe stack with clear evidence of top-to-the east shearing (figure 8) (Keller and Pialli, 1990; Keller et al., 1994; Collettini and Holdsworth, 2004).

The main facies of the Monte Capanne pluton exhibits a constant, peraluminous, monzogranitic composition (Poli et al., 1989; Dini et al., 2002; Gagnevin et al., 2004) while the mafic microgranular enclaves (MME) varies from tonalitic-granodioritic to monzogranitic. The

https://doi.org/10.5194/se-2021-11
Preprint. Discussion started: 16 February 2021

278 leucogranitic dykes are syenogranitic in composition (Gagnevin et al., 2004). Gagnevin et al.
279 (2004) proposed a multiphase magmatic emplacement from peraluminous magmas issued from
280 melting of a metasedimentary basement and hybridized with mantle-derived mafic magmas
281 whose heat supply possibly enhanced wall-rock assimilation. In addition, injection of mantle-
282 derived magma in the Sant' Andreas facies would have triggered extensive fractionation and
283 mixing of the basic magma with the resident monzogranitic mush (Poli and Tommasini, 1991).

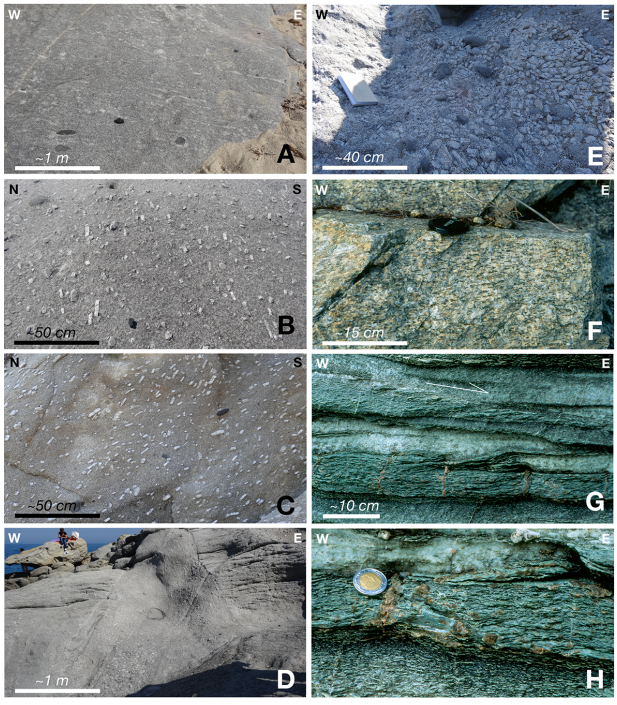

284

285 *Figure 7: Photographs of the Sant' Andrea facies in the Monte Capanne pluton and of the*
286 *deformation along the eastern margin of the pluton, in the pluton itself and in the contact*
287 *metamorphic aureole. A: general view of the orientation of K-feldspar megacrysts and some*
288 *mafic enclaves. B: Detailed view of the oriented K-feldspar megacrysts (horizontal plane). C:*
289 *zoom on the orientation of K-feldspar megacrysts (vertical plane). D: Cotoncello dyke. E:*
290 *cluster of K-feldspar megacrysts in the vicinity of the Cotoncello dyke. F: Mylonitic foliation*
291 *within the Monte Capanne shear zone. G: Sigmoidal foliation and top-to-the-east sense of*
292 *shear within the metamorphic aureole of the Monte Capanne pluton. H: detailed view of syn-*
293 *kinematic contact metamorphism garnets in veins perpendicular to the regional stretching*
294 *direction.*
295

https://doi.org/10.5194/se-2021-11
Preprint. Discussion started: 16 February 2021

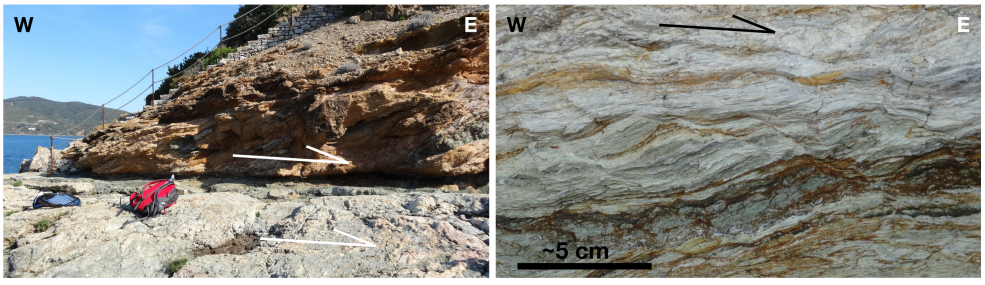

Figure 8: Photographs of the Zuccale detachment and its internal structure (see Collettini and Holdsworth, 2004). Upper: overview of the detachment fault. Lower left: Detail of the contact zone and the truncated foliation in the hanging wall. Lower right: detail of the shear bands indicating top-to-the east kinematics.

The internal magmatic structure of Monte Capanne pluton has been described based on the abundance of large alkali-feldspar phenocrysts (Farina et al., 2010). Three main facies corresponding to different magma batches emplaced within a too short period to be discriminated based on geochronology are reported with downward fining of grain size (figure 6). The largest grain size characterizes the upper Sant' Andrea facies that mainly crops out in the northwest of the pluton, while the finest grain size is observed in the lower San Piero facies cropping out mainly in its eastern part, within the zone affected by the most intense shearing. These three facies delineate an asymmetric dome-shaped bulk structure compatible with the general top-to-the east sense of shear. In the westernmost part of the Monte Capanne pluton near Sant' Andrea, mafic products are observed as large enclaves, with evidence of magma mixing and mingling. These mafic enclaves are mostly found in the Sant' Andrea facies that was emplaced first. Their occurrence in the westernmost part of the plutonic body, the farthest from the detachment, with a geometry similar to that observed on Serifos island in the Cyclades (Rabillard et al., 2015), suggests that they are associated with the root of the pluton.

Assuming that the three main felsic facies correspond to three successive intrusion batches, one observes an evolution toward finer grain size through time, an evolution that is compatible with progressive exhumation and also with a shorter residence time in the magma chamber, suggesting opening of the magmatic plumbing toward the surface leading to volcanic activity, as recorded above the detachment. The last episodes of intrusive activity are seen as a series of felsic dykes striking N-S or NE-SW, due to eastward extensional brittle deformation while the pluton was at near solidus conditions.

4.2. Orientation of K-feldpar megacrysts

https://doi.org/10.5194/se-2021-11
Preprint. Discussion started: 16 February 2021

325 A detailed study of the orientation of feldspar megacrysts was conducted along the shore
326 near Sant'Andrea (figures 7, 9, 10, 11). The pluton is there characterized by a high
327 concentration of megacrysts and of mafic enclaves reaching several meters in size. Megacrysts
328 show euhedral shapes in general.

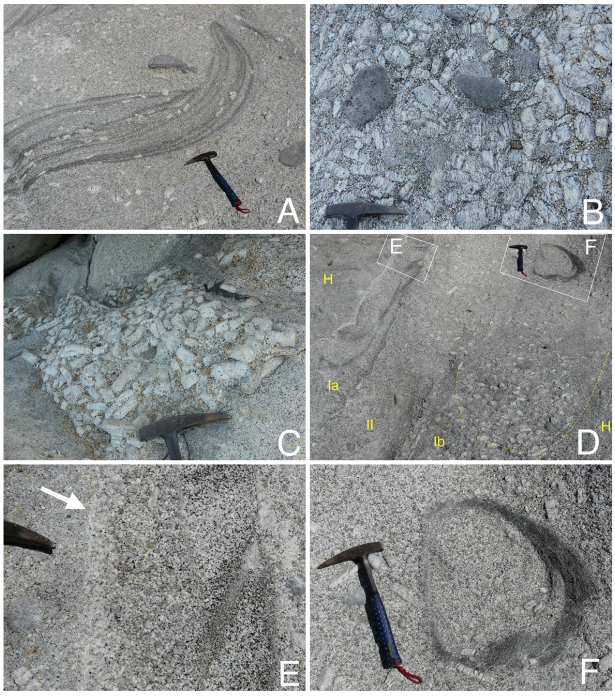

329

330 *Figure 9: Photographs of the root zone of the Sant'Andrea facies in the melange zone in and*
331 *around the Cotoncello dyke. A: Schlieren with cross-bedding. B: Mush zone with cluster of*
332 *K-feldspar megacrysts and mafic enclaves. C: Isolated blob of mush zone with large K-*
333 *feldspar megacrysts. D: Folded alternation of leucocratic and melanocratic layers with*
334 *schlierens. E: Detail of D, schlieren. F: detail of D: schlieren tube.*
335

336 Although the orientation of megacrysts is quite stable at the scale of a few hundred meters,
337 in the westernmost region the presence of the large enclaves is associated with a disorientation
338 of the megacrysts (figure 10A), indicating increasing tortuosity of the flow wrapping around
339 them associated with local turbulence in pressure shadows. Smaller enclaves are in general
340 aligned with the megacrysts. Some of the mafic enclaves with lobate shapes show a sharp
341 boundary with the felsic matrix, suggesting quenching of a hot mafic magma within the cooler
342 felsic magma (Fernandez and Barbarin, 1991; van der Laan and Wyllie, 1993; Fernandez and
343 Gasquet, 1994).
344

https://doi.org/10.5194/se-2021-11
Preprint. Discussion started: 16 February 2021

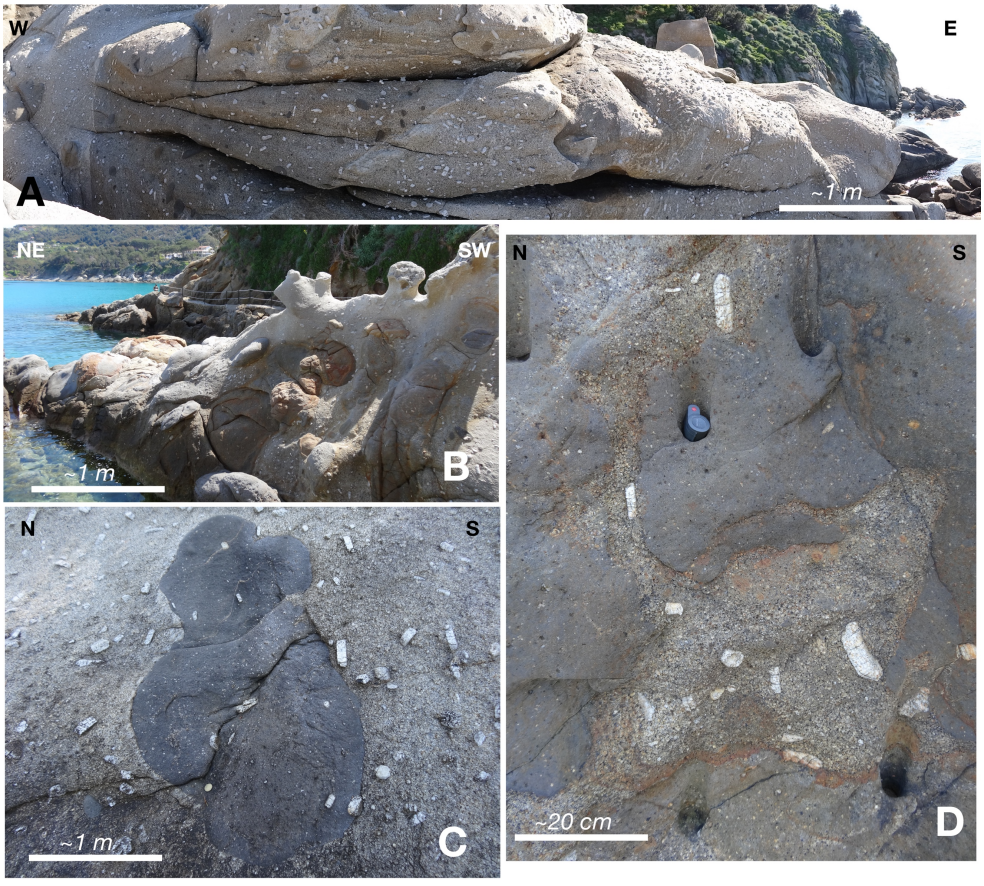

Figure 10: Photographs of large mafic enclaves and melange zones in the westernmost part of the Sant'Andrea facies showing the disorientation of K-feldspar megacrysts and melange facies (mingling).

Other enclaves are less mafic and show evidence of magma mingling-mixing. The disaggregation process of the mafic magma responsible of theses enclaves could happened either in a deep-seated magmatic chamber (Christofides et al., 2007), or more likely in the ascent conduit as a result of remelting of chilled mafic margins (Fernández and Castro, 2018) and subsequent viscous fingering dynamics (Perugini et al., 2005). Megacrysts contain inclusions of biotite, plagioclase and quartz and show euhedral shapes in general, although resorption surface has been noticed (Gagnevin et al., 2008). Other enclaves are less mafic and show evidence of magma mingling-mixing. These enclaves are associated with an aureole where feldspar crystals are concentrated, showing that the assimilation of the enclave occurred at the magmatic stage. Megacrysts are sometimes included within the mafic enclaves, showing that they were already present before the solidification of enclaves and thus providing evidence

https://doi.org/10.5194/se-2021-11
Preprint. Discussion started: 16 February 2021

of low viscosity contrast between the enclaves and the host magma at the magmatic stage. All these observations suggest that this western zone is a mixing between a mafic magma of mantle origin and a felsic magma partly issued from crustal anatexy and that this part of the pluton is close to the main feeder. This conclusion is confirmed by AMS (anisotropy of magnetic susceptibility) showing that the magnetic foliation and lineation are steeper there than anywhere else in the pluton (Bouillin et al., 1993).

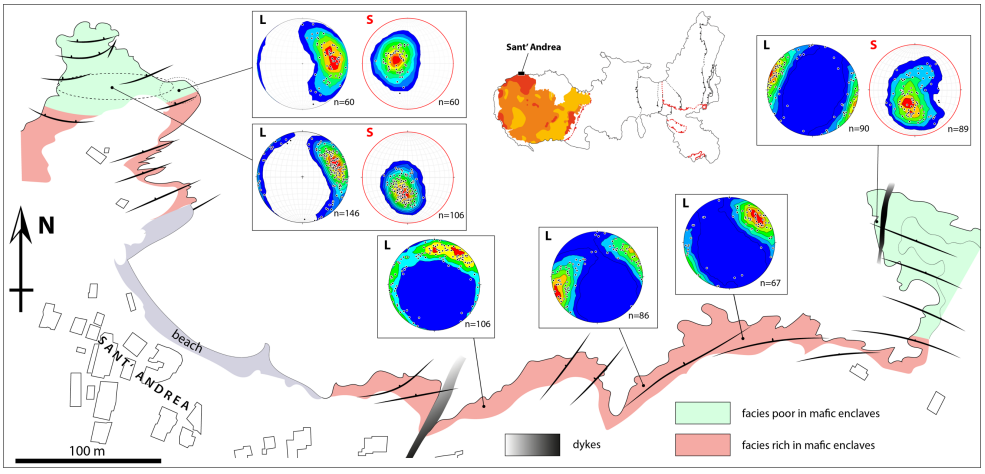

Figure 11: Detailed study of the orientation of K-feldspar megacrysts in the Sant-Andrea facies with foliation trajectories.

Further to the east, still within the Sant' Andrea facies, the main granite is intruded by a N-S syeno-granitic dyke-like structure near Cotoncello headland, made of a finer-grained facies and a lower concentration of megacrysts and enclaves (figure 7D, figure 9). In its vicinity, the host granite contains folded schlierens with cross-bedding (Figure 9A). Within these large schlierens, the megacrysts are aligned parallel with the folded foliation of biotite-rich layers. From place to place, decametric megacryst-rich mush zones enriched in decametric and rounded mafic enclaves occur in this host facies (Figure 9B). In addition, isolated blobs of mush, characterized by an irregular shape, are observed in the coarse-grained, megacryst-poor domains (Figure 9C). These blobs originate from the disruption of preexisting mush zones within the root zone by subsequent magma injection as illustrated by the dyke-like structure (Rodríguez and Castro, 2019). This structure is composed of three successive injections characterized by undulating and fuzzy boundaries (Figure 9D). The westernmost injection (injection Ia, figure 9D) shows folded alternating leucocratic flow-sorted layers made of quartz, K-feldspar and plagioclase with more melanocratic layers rich in biotite that can be described as schlierens (Figure 9E). These schlierens are folded and cross-cut by a subsequent and final

https://doi.org/10.5194/se-2021-11
Preprint. Discussion started: 16 February 2021

injection (Figure 9D, injection II). In the easternmost injection (Figure 9D, injection Ib), K-feldspar megacrysts are accumulated and their orientation defines a concave upwards foliation. Such mineral fabric is similar to those described by Rocher et al. (2018) in finger and drip structures developed at the margins of the Asha pluton (NW Argentina) and interpreted as mechanical accumulation in a downward localized multiphase magmatic flow. In addition, this megacrysts accumulation is associated at its top with ring schlieren that could represent a cross-section of a schlieren tube (e.g. Žák and Klomínský, 2007) (figure 9F). Ring schlierens are also associated with drip structures in the Asha pluton among others (Paterson, 2009; Rocher et al., 2018). The most external rim between the host body H and injection Ia (Figure 9D) is associated with a reaction zone with recrystallization of quartz and K-felspar (Figure 9E, white arrow). Outside the injections, the mineral fabric shown by the K-feldspar megacrysts tends to reorientate parallel to the rims.

All these observations point out to an injection of a low viscosity, crystal poor, magma with a viscosity contrast of about one order of magnitude lower with respect to its host magma (Wiebe et al., 2017). Mineral fabrics and accumulation, folded and ring schlieren indicate that the structures were formed by localized multiphase magmatic flow when the crystallizing host magma remained partially molten, probably containing around 50% of crystals (Weinberg et al., 2001). The Cotoncello dyke-like structure is thus co-magmatic with the Sant'Andrea facies, but the pluton was already enough crystallized to allow the formation of N-S cracks in the crystal mush capable of transmitting tectonic stress where the magma was injected.

Between the Cotoncello dyke and the root zone to the west, the proportion of enclaves and megacrysts is everywhere high. Systematic measurements of felspar megacrysts were made (figure 11). Mineral foliation and lineation represents the main orientation distributions of the orientation of (010) faces and [001] major axis of the measured crystals, respectively. At the scale of a few hundred meters the fabric shows a consistent pattern with a low-angle north-dipping foliation more prominent in regions poorer in mafic enclaves. The lineation is in average E-W trending. Late mafic and acidic dykes strike perpendicular to the lineation. Within the mélange zone, the mineral fabric is often perturbated approaching enclave swarms. Then, the fabric becomes more uniform with variations around an average ENE-WSW trend from N30 to N100°E for the long axes of megacrysts.

As the megacrysts were formed in early magmatic conditions (Vernon, 1986; Vernon and Paterson, 2008), they were in suspension within the melt. Such a preferential orientation is due to a rigid rotation of isolated crystals within a viscous matrix submitted to magmatic flow (Fernandez and Laporte, 1984). In the present case, the various observations attesting for a co-

https://doi.org/10.5194/se-2021-11
Preprint. Discussion started: 16 February 2021

magmatic fabric show that the preferential orientation of the megacrysts foliation results from a fossilization of the magmatic flow. The large-scale variations of the foliation attitude suggest in addition that the E-W to ENE-WSW flow was laminar in general, except in the immediate vicinity of the large enclaves where the flow wrapping around these stronger bodies was more turbulent.

These detailed observations show that the internal magmatic fabric of the pluton is similar in orientation with its overall tectonic fabric, including the sub-solidus deformation along the eastern margin due to the detachment with a main stretching direction oriented WNW-ESE, as shown by magnetic susceptibility studies (Bouillin et al., 1993) and deformation features near the main eastern contact within the eastern extensional shear zone (Daniel and Jolivet, 1995). This focussing of the pluton fabric, from the magmatic stage to the brittle stage around an E-W stretching direction compatible with the extensional shear along the main detachment, suggests that the magmatic flow was oriented parallel to the main direction of extension active at crustal scale since the magmatic stage. A continuum is thus observed from the magmatic stage to the sub-solidus deformation and the localization of the detachment, and this continues during the emplacement of the younger Porto-Azzuro pluton and the formation of the Zuccale low-angle normal fault. This evolution recalls that of the Aegean plutons summarized above.

5. Discussion and modelling

5.1. Synthesis of observations

The coaxiality of the structures measured in the Monte Capanne pluton from its magmatic stage to the tectonic overprint is similar to observations made on the Cycladic plutons, especially Ikaria and Serifos where a similar gradual transition is observed from the magmatic stage to the localisation of strain along the main detachment. The similarity goes further as the root of the pluton shows a mixture of mafic and felsic facies. On Serifos (figure 4), field observations show that the root of the pluton is characterized by vertical or steep dykes and some of them are dilacerated by the top-south flow while the magma is still viscous (Rabillard et al., 2015). Moving toward the detachment, the sub-solidus deformation takes over with a N-S trending stretching lineation and top-south kinematic indicators. A similar evolution can be observed in the Raches pluton of Ikaria island in the Cyclades (Laurent et al., 2015). Emplaced below to top-to-the north detachment, the magma shows a steep foliation in the south far from

https://doi.org/10.5194/se-2021-11
Preprint. Discussion started: 16 February 2021

453 the detachment and it flattens toward the north to become parallel to the detachment plane.
454 Evidence of co-magmatic stretching and shearing parallel to the regional stretching direction is
455 observed in the southern side of the pluton and sub-solidus mylonitization and ultra-mylonites
456 on the northern side. A similar situation can be described in the case of the Naxos granodiorite
457 (Bessière et al., 2017). All cases show the syn-kinematic character of the pluton, the best
458 evidence being the syn-kinematic contact metamorphism.

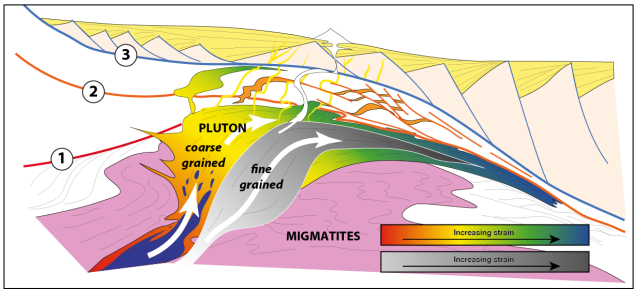

459
460 *Figure 12: Schematic section showing a conceptual model of the relations between syn-*
461 *kinematic plutons and the detachments, based on the examples of the Aegean and North*
462 *Tyrrhenian plutons. Modified from Rabillard et al. (2018).*
463

464 The Monte Capanne pluton thus shows clear similarities with the Aegean plutons. Figure
465 12 shows a simplified scheme of the geometrical and kinematic relations between detachments
466 and plutons based on the examples of the Aegean and the Northern Tyrrhenian, modified from
467 Rabillard et al. (2018). The root zone of the pluton, characterized with an association of mafic
468 and acidic magmas, shows a steeper upward magmatic flow and evidence of co-magmatic
469 stretching and shearing parallel to the regional direction of extension with a kinematics similar
470 to that of the main detachments. During the emplacement of the pluton, the magma chamber
471 progressively opens toward the surface and the granitoids evolve toward finer-grained facies.
472 Progressive extension and exhumation is accompanied by the inflation of the pluton and
473 injection of dykes across the ductile detachment. New detachments are formed above
474 sequentially.
475

476 ### 5.2. *A conceptual model based on published numerical experiments*
477

478 This evolution can be compared with numerical models. Thompson and Connolly (1995)
479 summarize the three ways of melting lower continental crust as (1) supplying water to the crust
480 to lower the solidus, (2) decreasing pressure and (3) providing additional heat to the lower crust.
481 They also state that extension alone of a thickened crust is unlikely to reach the conditions of

https://doi.org/10.5194/se-2021-11
Preprint. Discussion started: 16 February 2021

lower crustal melting unless some additional heat is given by the mantle. Back-arc regions above retreating slabs, where the lithosphere is thinned and the asthenosphere advected upward underneath the crust seem to the first order to fit these conditions (Roche et al., 2018).

Schubert et al. (2013) have explored numerically the effect of the injection of molten mafic material in an extending crust. They show that the injection of this hot material in the lower crust will induce melting and trigger the formation of felsic magmas that will then ascent along steep normal faults all the way to the upper crust, forming the observed plutons. This is a situation that can easily be compared with the Aegean or the Tuscan archipelago where the granitoids are associated in their root zones with coeval mafic magmas and the felsic plutons ascend along low-angle detachments. In figure 13, we propose a further conceptual model based on numerical experiments of post-orogenic extensional deformation with low-angle shear zones (Huet et al., 2011).

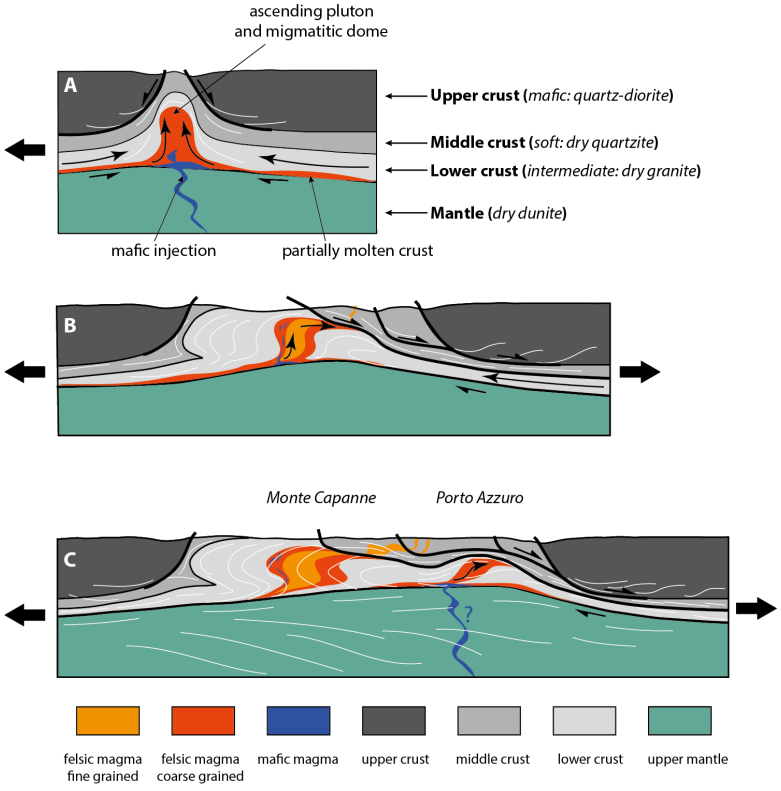

Figure 13: Conceptual model of the succession of events leading to the emplacement of a plutonic system below an active series of detachments, based on Huet et al. (2011) and Schubert et al. (2013).

https://doi.org/10.5194/se-2021-11
Preprint. Discussion started: 16 February 2021

In this series of numerical experiments, the thermal gradient and Moho temperature were varied as well the rheological stratification with either a classical rheological stratification or an inverted crustal structure resulting from the formation of the pre-extension nappe stack, the latter setup being used in figure 13, see also Labrousse et al. (2016) for more details on the dynamics of this system with inverted rheological profiles. This latter choice is designed to mimic the Aegean orogenic wedge where the Cycladic Blueschists Unit is sandwiched between the Cycladic Basement and the Upper Cycladic Unit (UCU) (Huet et al., 2009; Jolivet and Brun, 2010; Ring et al., 2010). The UCU belongs to the Pelagonian paleogeographic domain and is largely composed of an ophiolite, denser and stronger than the CBU (Labrousse et al., 2016) as well as other basement lithologies (Reinecke et al., 1982; Katzir et al., 1996; Soukis and Papanikolaou, 2004; Martha et al., 2016; Lamont et al., 2020). Asymmetric lateral boundary conditions are applied with 1 cm/yr on the left side and no displacement of the right side as in Tirel et al. (2004). The upper surface is free and the base is driven by hydrostatic forces. No prescribed discontinuity is introduced in the model, strain localization is only due to the use of random noise in the cohesion value of the upper crust (for more details, see Huet et al., 2011). The results shown here represent a case where the rheological stratification is inverted and the thermal gradient is high, a likely situation in the Aegean or Tyrrhenian post-orogenic and back-arc contexts.

The conceptual model of the interactions between the numerical model dynamics and the intrusions is that we assume that a batch of mafic magmas, issued from partial melting of the mantle, is injected at the base of the lower crust where it triggers the melting of felsic materials. This leads to the formation of migmatites and collection of the felsic melts in a rising pluton progressively caught in the detachment dynamics as it reaches the upper parts of the crust. The felsic magma is thus deformed while it is still partly liquid and then mylonitized once it has cooled down below the solidus. While extension proceeds, the overburden is removed by the activity of the detachment and the molten material that comes next is injected in lower pressure conditions and finds a faster access to the surface because of extension, thus leading to smaller grainsize plutonic facies and probable volcanism at the surface. While the system of detachments migrates toward the right and a new dome forms, the same situation can be reproduced and a new pluton is emplaced below a detachment further to the right, closer to the active detachment. This evolution is reminiscent of the evolution of Elba Island with the formation of the Monte Capanne pluton in a first stage and the Porto Azzuro pluton in a later stage.

https://doi.org/10.5194/se-2021-11
Preprint. Discussion started: 16 February 2021

5.3. *Testing the concept with numerical experiment*

This conceptual model is now tested with new numerical experiments involving the emplacement of magmas like in Schubert et al. (2013), but in a different situation where low-angle detachments form, to see whether the introduction of a low-viscosity material in the model developed by Huet et al. (2011) would drastically change the system dynamics or not. This has been done for figures 14, 15 and 16.

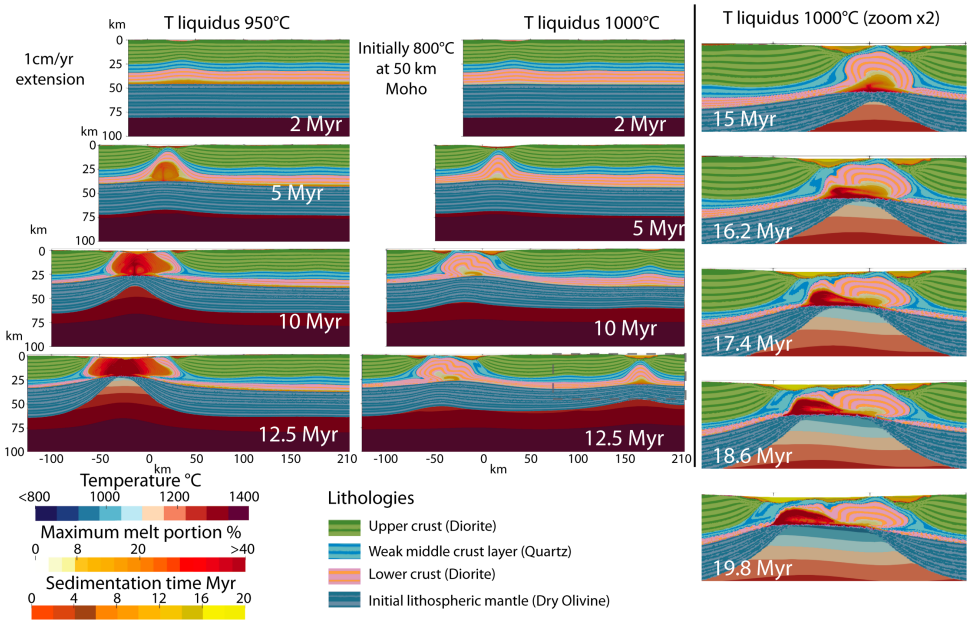

Figure 14: Snapshots of the numerical experiments with two different liquidus temperatures (950°C and 1000°C) from 2 to 12.5 Myr. White line limits the molten lower crust with melt ration above 40% (pluton).

The kinematics of exhumation produced by the nappe stacking experiments of Huet et al. (2011) produces extension along long-lived detachment better resembling Mediterranean example than diapiric spreading models that are produced by models with no intermediate weak layers as in Tirel et al. (2004, 2008) or Rey et al. (2009). Hence, in order to test how molten rocks interacts with detachments, we decided to build on our experience and start from this set up which is a 210 km wide model domain submitted to 1cm/yr of extension on its left side for 10 Myr or more with an initial lithospheric column constituted from 25 km upper crust, 10 km weak middle crust, 15 km thick lower crust overlying 40 km of lithospheric mantle. The Moho located at 50 km depth is initially at a temperature of 830°C. We have taken the same

https://doi.org/10.5194/se-2021-11
Preprint. Discussion started: 16 February 2021

555 rheological parameters which are reported in Table A1 (Appendix A). The four major
556 differences with Huet et al. (2011) are :
557
558 i) Erosion and sedimentation applied on the top boundary,
559 ii) the deforming Wrinkler foundation at the LAB has been replaced by inflow of
560 asthenospheric material with higher thermal diffusivity to simulate small scale
561 convection and keep the base of the lithosphere at 1300°C during the experiments
562 as it was the case in Huet et al. (2011) study,
563 iii) the numerical code used in this study is pTatin2d (May et al., 2014, 2015) that solves
564 the same momentum equation

565 $$\nabla . \sigma = \rho g$$

566 For velocity *v*, as well as heat conservation
567

568 $$-\nabla . (-\kappa \nabla T + vT) + H = \frac{\partial T}{\partial t}$$

569
570 for Temperature T as Huet et al. (2011). However, it uses an incompressible visco-plastic
571 rheology minimizing the stress between a dislocation creep regime and Drucker Prager failure
572

573 $$\nabla . v = 0$$
$$\sigma = min\left(\sin\phi + 2\,C\cos\phi\,, \dot{\varepsilon}^{\frac{1}{n}} A^{\frac{-1}{n}} e^{\frac{Q+VP}{nRT}}\right)$$

574
575 to evaluate an effective viscosity :

576 $$\eta_r = \frac{\sigma}{2\dot{\varepsilon}}.$$

577
578 instead of visco-elasto-plastic rheology based on dislocation creep and Mohr Coulomb failure
579 criteria.
580
581 iv) We added a simplified parametrization in order to account for the mechanical effect
582 of a melt in the simulations. The melt fraction M_f has been introduced as a linear
583 function of solidus (T_s) and liquidus (T_l) temperature
584

585 $$M_f = \min\left(max\left(\frac{T - T_s}{T_l - T_s}, 0\right), 1\right)$$

https://doi.org/10.5194/se-2021-11
Preprint. Discussion started: 16 February 2021

following Gerya and Yuen (2003). Based on melt fraction, the density and viscosity of passive markers are modified following algebraic averaging for density

$$\rho = M_f \rho_m + (1 - M_f)\rho_r,$$

and harmonic averaging for viscosity

$$\eta = \left(\frac{M_f}{\eta_m} + \frac{1-M_f}{\eta_r}\right)^{-1}.$$

The solidus dependence on pressure P (in GPa) is implemented following wet granite solidus of Miller et al. (2003), but we also added a variable temperature offset ΔT to account for more mafic granitic composition as follows:

$$T_s^c = 590 + \frac{250}{10(P + 0.1)} + \Delta T$$

and the dependence of liquidus to pressure is modeled following:

$$T_l^c = T_s^c|_{P=0} + 10 + 200P.$$

The mantle is also allowed to melt following Hirshmann et al. (2000) solidus law

$$T_s^m = -5.904P^2 + 139.44P + 1108.08$$
$$T_l^m = T_s^m + 600$$

All solidus and liquidus are represented on figure A2 (Appendix A) as a function of pressure and temperature. For low melting temperature of the lower crust (wet granite solidus with ΔT up to 100°C), the crust is largely molten in the initial conditions and buoyancy effects dominate forming "spreading domes" in the classification of Huet et al. (2011), and this despite the presence of a weak middle crustal layer. For higher melting temperature (ΔT from 150°C) melt proportion remains below the 8% melt connectivity threshold described by Rosenberg and Handy (2005) during most of the simulation. We interpret elements with markers that never

https://doi.org/10.5194/se-2021-11
Preprint. Discussion started: 16 February 2021

618 crossed that critical threshold as migmatites. In that case, melting does not disrupt the typical
619 asymmetric detachment kinematics observed in Elba and in the Cyclades that was well
620 reproduced by Huet et al. (2011) study. In the late stage of deformation, when the lithospheric
621 mantle is sufficiently attenuated by boudinage, the temperature of the lower crust reaches a
622 sufficient temperature to melt more generously, generating plutons which we define as markers
623 with a melt proportion greater than 40%.

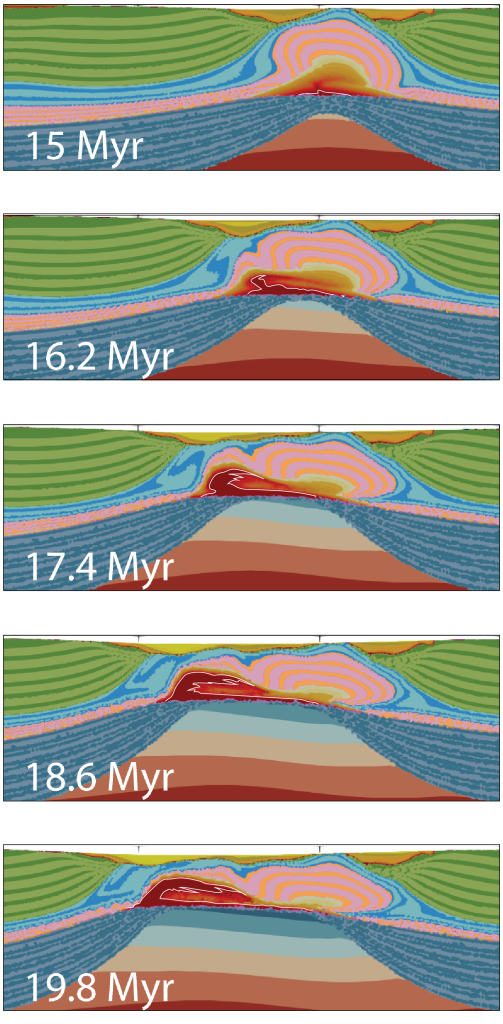

624
625 *Figure 15: Zoom of the last 5 Ma of evolution of the model of figure 15 with a liquidus*
626 *temperature of 1000°C from 15Myr to 19.8 Myr (black dotted rectangle on figure 15 for*
627 *location).*
628
629

https://doi.org/10.5194/se-2021-11
Preprint. Discussion started: 16 February 2021

With a temperature of 950°C at the surface for the liquidus, the molten layer is initially thicker (figure 14) and strain develops into a spreading dome geometry like in the models of Tirel et al. (2004, 2008) or Rey et al. (2009), with symmetric strain pattern and limited strain localization. Shear is indeed progressively relocalized on newly formed shear zones at the top of newly exhumed hot material at the structure axis. When the temperature of the liquidus is higher, reaching 1000°C in surface conditions (figure 14), the molten layer is initially thinner, the deformation is persistently more localized on a detachment on one edge of the dome structure and the model evolves with a detachment on the side of a dome with a limited rate of partial melting in the lower crust (<8%). The deformation ultimately migrates to form a second dome where a syn-kinematic low viscosity body develops with a melt ratio >40%, which we interpret as analogous to a granite intrusion. The late evolution of this second dome shows a strongly asymmetric geometry with the shape of the syn-kinematic intrusion controlled by the asymmetry in strain pattern and a low-angle shear zone (figure 15). Figure 16 shows a structural interpretation of the final step of the model for the second dome highlighting this asymmetry: the dome is bounded by two antithetic crustal scale persistent shear zones, with steep and shallow dip, and an eccentricity of the intrusion feeding pipe within the dome. This overall asymmetrical strain and intrusion localization in the case of limited partial melting rate hence reproduces the main features of the strain and intrusion pattern described in the field in the Cyclades and Elba.

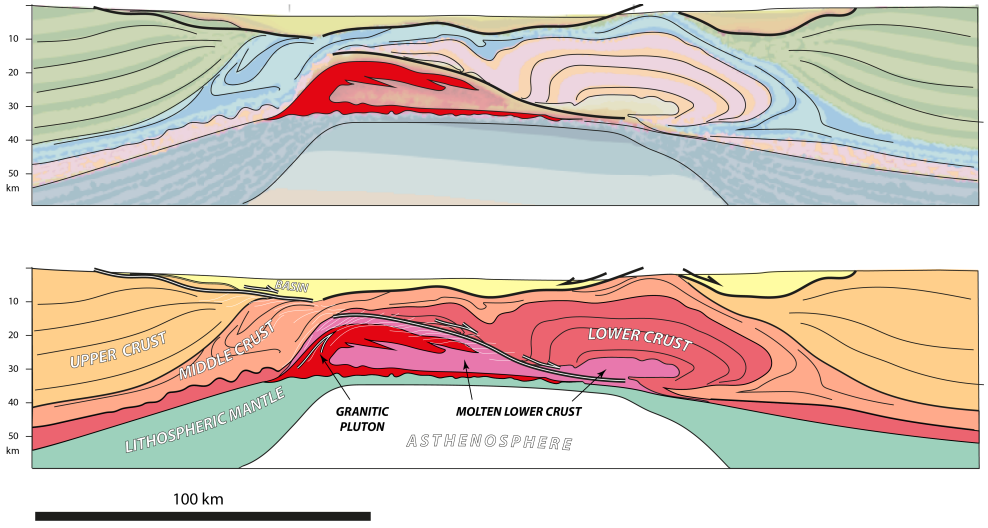

Figure 16: Structural cross-section based on the most evolved stage of the numerical model at 19.8 Myr.

https://doi.org/10.5194/se-2021-11
Preprint. Discussion started: 16 February 2021

653

654 Although the model does not show the details of the interactions between the dome and
655 the pluton, which involve percolation of melts, drainage through migmatites and dyke-swarms,
656 and progressive intrusion of the detachment by the rising granite, the overall geometry and
657 kinematics is similar with the natural case. The observed geometry is better reproduced in runs
658 with higher crustal melting temperatures and limited melt production. Low temperature melting
659 reactions for the continental crust are the wet solidus and the muscovite dehydration solidus,
660 while biotite and hornblende dehydration melting reactions could represent higher temperature
661 melting reactions (Weinberg and Hasalová, 2015). The model does not show either the role of
662 mafic injections at the base of the model. In the case of the Aegean and Monte Capanne, we
663 have postulated that mafic melts, generated by partial melting of the mantle in the arc and back-
664 arc region, intrude the lower crust and trigger the generation of felsic melts that then rise within
665 the dome. This is an additional input of heat in the model that would also localize the weakest
666 layers and thus the deformation and likely favor the evolution of the model in the same direction
667 as in the model presented here with a lower melting temperature. Similar evolution can arise
668 with an additional input of water in the lower crust. This water may originate from amphibole-
669 rich gabbros (sanukitoides) that could act as water donors enhancing lower crustal partial
670 melting to further produce secondary I-type granites (Castro, 2020). In the Aegean arc, whereas
671 amphibole bearing, I-type granites (Naxos and Serifos granodiorites among others) likely
672 reassemble secondary I-type granites as described by Castro et al. (2020 and references therein),
673 this water origin remains elusive as amphibole-bearing mantle magmas are not yet evidenced
674 interacting with the migmatites, except in the Mykonos-Delos-Rheneia MCC (Jolivet et al.,
675 2021).

676 The metamorphic parageneses associated with contact metamorphism in the case of Elba
677 suggests a depth of emplacement of the pluton of 4-5 km. In the numerical model, the genesis
678 of the pluton starts in the lower crust at a larger depth. The contact metamorphism observed in
679 the field characterizes the upper part of the pluton after it had risen within the crust, which may
680 explain this apparent contradiction.

681 One additional factor has not been considered in this study, the heterogeneity of the crust
682 inherited from earlier tectonic events. It has been shown by numerical experiments that dipping
683 heterogeneities in the crust mimicking structures inherited from nappe stacking help localizing
684 deformation, favoring the development of asymmetrical extensional structures and the
685 development of MCCs (Le Pourhiet et al., 2004; Huet et al., 2011; Lecomte et al., 2011; 2012).
686 Using this sort of initial conditions with melting would also favor the localization of

https://doi.org/10.5194/se-2021-11
Preprint. Discussion started: 16 February 2021

687 deformation on a single detachment. It may alternatively favor the development of several
688 asymmetric domes with low-angle detachments. Future studies should focus on testing such
689 initial conditions and also test these processes in 3-D.
690 The comparison of the Aegean and North Tyrrhenian plutons shows that the model of
691 interactions between plutons and detachments proposed by Rabillard et al. (2018) is
692 reproducible in similar contexts in different regions and can thus be probably generalized. The
693 comparison of this field-based conceptual model with numerical models moreover suggests that
694 this conceptual model is physically feasible. It requires the concomitance of post-orogenic
695 extension, thus extension set on an orogenic wedge, and a back-arc context to provide the
696 necessary heat and water for the generation of magmas in the mantle and the crust. The
697 possibility of a slab tear would be even more favorable as it increases the possibilities of
698 advecting hot asthenosphere directly below the extending crust (Roche et al., 2018).
699 As shown in the 3-D numerical experiments of Roche et al. (2018), slab retreat and back-
700 arc extension lead to the boudinage of the lithosphere with a spacing of ~100 km which will
701 then localize the formation of crustal domes and detachments. This type of evolution may
702 explain the formation of the lines of domes observed in the Aegean and the Menderes Massif.
703 Whether the boudinage also focuses the collection of mantle-derived magmas below the domes
704 is a question that should be addressed by further modelling. This question is important also
705 because the interactions between plutons and detachments described here and in Rabillard et
706 al. (2018) may provide guides for geothermal exploration. The case of the Menderes Massif is
707 exemplary of the intimate relations between active geothermal fields and crustal-scale
708 detachments (Roche et al., 2018). The case of the Tuscan Archipelago is partly similar with the
709 geothermal fields of Larderello and Monte Amiata developed above recent shallow plutons in
710 a context of asymmetric extension with top-to-the east low-angle shear zones (Jolivet et al.,
711 1998; Brogi et al., 2003; Rochira et al., 2018). The Monte Capanne and Porto Azzuro plutons
712 on Elba are associated with hydrothermal activities and mineralization (Maineri et al., 2003;
713 Rossetti and Tecce, 2008; Liotta et al., 2015) that make them good exhumed analogues of active
714 geothermal fields, a situation that is found also in the Cyclades with the mineralizations
715 observed on Mykonos or Serifos in the Cyclades (Salemink, 1985; St. Seymour et al., 2009;
716 Menant et al., 2013; Tombros et al., 2015; Ducoux et al., 2016).
717

718 ## 6. Conclusions
719

https://doi.org/10.5194/se-2021-11
Preprint. Discussion started: 16 February 2021

The comparison between the Aegean and Tyrrhenian Miocene plutons shows striking similarities in their interactions with coeval detachments. These plutons were all emplaced underneath low-angle ductile shear zones and brittle detachments in a post-orogenic back-arc environment where extra heat is provided by advected asthenospheric mantle. The roots of those felsic plutons show a mixing with mafic magmas. The magmatic fabric is steep in the vicinity of the roots and shallows toward the detachments. The plutons record substantial stretching and shearing coaxial with the regional deformation while they still contain a significant amount of melt. In sub-solidus conditions, the granitoids are then mylonitized when approaching the detachment, until the formation of ultra-mylonites and pseudotachylytes. In both cases too, the felsic magma intrudes the detachment and invades the upper plate. A migration of detachments is then observed from the deep and ductile detachments to more brittle and surficial ones. Late magmatic batches show a smaller grain size compatible with an opening of the magma chamber toward the surface suggestive of the volcano-plutonic context of these plutons. To account for these similarities suggesting that this model can be generalized we proposed a conceptual model where mafic magmas batches are injected in the lower crust of an extending orogenic wedge in a back-arc region with low-angle detachments. These mafic injections trigger the melting of the lower crustal felsic material and the ascent of felsic plutons in the crust, controlled by the low-angle detachments. The migration of the detachments through time explains the migration of plutons and detachments observed in the Tuscan Archipelago and in Tuscany from the Late Miocene to the Late Pliocene, as well as in the Aegean. This conceptual model is tested with a numerical approach showing the impact of melt supply in the development of the dome strain pattern. The observed asymmetry of strain localization and intrusion are reproduced for a limited melting rate, while a higher melting rate would lead to the development of a completely different dome structure. The geometry and kinematics observed in the field are well reproduced by the model. These intimate interactions between plutons and detachments can be foreseen as useful guides for the prospection and understanding of geothermal and associated mineralization.

Author contribution: Laurent Jolivet, Laurent Arbaret, Florent Cheval-Garabedian, Vincent Roche and Aurélien Rabillard did the field work in the Aegean, Loïc Labrousse and Laetitia Le Pourhiet designed the modeling procedure and ran the numerical experiments. All authors contributed to the writing of the manuscript.

Competing interests: The authors declare that they have no conflict of interest.

https://doi.org/10.5194/se-2021-11
Preprint. Discussion started: 16 February 2021

752 **Acknowledgments**: This paper is a contribution of the ERC Advanced Research Grant
753 RHEOLITH (grant agreement No.290864), of Institut Universitaire de France and Labex
754 VOLTAIRE.

755 References

756

757 Angelier, J., Glaçon, G., Muller, C., 1978. Sur la présence et la position tectonique du Miocène
758 inférieur marin dans l'archipel de Naxos (Cyclades, Grèce). C. R. Acad. Sc. Paris 286,
759 21-24.
760 Avanzinelli, R., Lustrino, M., Mattei, M., Melluso, L., Conticelli, S., 2009. Potassic and
761 ultrapotassic magmatism in the circum-Tyrrhenian region: Significance of carbonated
762 pelitic vs. pelitic sediment recycling at destructive plate margins. Lithos 113, 213–227;
763 doi:210.1016/j.lithos.2009.1003.1029.
764 Barberi, F., Giglia, G., Innocenti, F., Marinelli, G., Raggi, G., Ricci, C.A., Squarci, P., Taffi,
765 L., Trevisan, L., 1967. Carta geologica dell' isola d'Elba scala 1:25000. C.N.R. Roma.
766 Bargnesi, E.A., Stockli, D.F., Mancktelow, N., Soukis, K., 2013. Miocene core complex
767 development and coeval supradetachment basin evolution of Paros, Greece, insights from
768 (U–Th)/He thermochronometry. Tectonophysics 595-596, 165-182,
769 dx.doi.org/110.1016/j.tecto.2012.1007.1015.
770 Beaudoin, A., Augier, R., Laurent, V., Jolivet, L., Lahfid, A., Bosse, V., Arbaret, L., Rabillard,
771 A., Menant, A., 2015. The Ikaria high-temperature Metamorphic Core Complex
772 (Cyclades, Greece): Geometry, kinematics and thermal structure. Journal of
773 Geodynamics 92, 18-41, http://dx.doi.org/10.1016/j.jog.2015.1009.1004.
774 Berger, A., Schneider, D.A., Grasemann, B., Stockli, D., 2013. Footwall mineralization during
775 Late Miocene extension along the West Cycladic Detachment System, Lavrion, Greece.
776 Terra Nova 25, 181-191, doi: 110.1111/ter.12016.
777 Berthé, D., Choukroune, P., Jegouzo, P., 1979. Orthogneiss, mylonite and non coaxial
778 deformation of granites : the example of the South Armorican Shear Zone. J. Struct.
779 Geol. 1, 31-42.
780 Bessière, E., Rabillard, A., Précigout, J., Arbaret, L., Jolivet, L., Augier, R., Menant, A.,
781 Mansard, N., 2017. Strain localization within a syn-tectonic intrusion in a back-arc
782 extensional context: the Naxos monzogranite (Greece). Tectonics 37, DOI:
783 10.1002/2017TC004801.

https://doi.org/10.5194/se-2021-11
Preprint. Discussion started: 16 February 2021

784 Bianco, C., Brogi, A., Caggianelli, A., Giorgetti, G., Liotta, D., Meccheri, M., 2015. HP-LT
785 metamorphism in Elba Island: Implications for the geodynamic evolution of the inner
786 Northern Apennines (Italy). Journal of Geodynamics 91, 13-25;
787 http://dx.doi.org/10.1016/j.jog.2015.1008.1001.
788 Bianco, C., Godard, G., Halton, A., Brogi, A., Liotta, D., Caggianelli, A., 2019. The lawsonite-
789 glaucophane blueschists of Elba Island (Italy). Lithos 348-349, 105198;
790 https://doi.org/105110.101016/j.lithos.102019.105198.
791 Bolhar, R., Ring, U., Allen, C.M., 2010. An integrated zircon geochronological and
792 geochemical investigation into the Miocene plutonic evolution of the Cyclades, Aegean
793 Sea, Greece: Part 1: Geochronology. Contrib Mineral Petrol 160, 719–742, DOI
794 710.1007/s00410-00010-00504-00414.
795 Bolhar, R., Ring, U., Kemp, A.I.S., Whitehouse, M.J., Weaver, S.D., Woodhead, J.D., Uysal,
796 I.T., Turnbull, R., 2012. An integrated zircon geochronological and geochemical
797 investigation into the Miocene plutonic evolution of the Cyclades, Aegean Sea, Greece:
798 part 2: geochemistry. Contr. Miner. Petrol. 164, 915-933.
799 Bonin, B., 2004. Do coeval mafic and felsic magmas in post-collisional to within-plate regimes
800 necessarily imply two contrasting, mantle and crustal, sources? A review. Lithos 78 1–
801 24; doi:10.1016/j.lithos.2004.1004.1042.
802 Bouillin, J.P., Bouchez, J.L., Lespinasse, P., Pêcher, A., 1993. Granite emplacement in an
803 extensional setting: an AMS study of the magmatic structures of Monte Capanne (Elba,
804 Italy). Earth and Planetary Science Letters 118, 263-279.
805 Bouillin, J.P., Poupeau, G., Sabil, N., 1994. Etude thermo-chronologique de la dénudation du
806 pluton du Monte Capanne (île d'Elbe, Italie) par les traces de fission. Bulletin de la Société
807 Géologique de France 165, 19-25.
808 Brogi, A., Lazzarotto, A., Liotta, D., Ranalli, G., 2003. Extensional shear zones as imaged by
809 reflection seismic lines: the Larderello geothermal field (central Italy). Tectonophysics
810 363, 127-139.
811 Brown, M., 1994. The generation, segregation, ascent and emplacement of granite magma: the
812 migmatite-to-crustally-derived granite connection in thickened orogens. Earth-Science
813 Reviews 36, 83-130.
814 Brown, M., 2007. Crustal melting and melt extraction, ascent and emplacement in orogens :
815 mechanisms and consequences. J. Geol. Soc London 164, 709-730.
816 Brown, M., Solar, G.S., 1998. Shear-zone systems and melts: feedback relations and self-
817 organization in erogenic belts. J. Struct. Geol 20, 211-227.

https://doi.org/10.5194/se-2021-11
Preprint. Discussion started: 16 February 2021

818 Brunet, C., Monié, P., Jolivet, L., Cadet, J.P., 2000. Migration of compression and extension in
819 the Tyrrhenian Sea, insights from 40Ar/39Ar ages on micas along a transect from Corsica
820 to Tuscany. Tectonophysics 321, 127-155.
821 Buick, I.S., 1991. The late alpine evolution of an extensional shear zone, Naxos, Greece. J.
822 Geol. Soc. 148, 93-103; doi:110.1144/gsjgs.1148.1141.0093.
823 Buick, I.S., Holland, T.J.B., 1989. The P-T-t path associated with crustal extension, Naxos,
824 Cyclades, Greece, in: Daly, J.S. (Ed.), Evolution of metamorphic belts, pp. 365-369;
825 doi:310.1144/GSL.SP.1989 .1043.1101.1132.
826 Camelli, G.M., Dini, I., D, L., 1993. Upper crustal structure of the Larderello geothermal field
827 as a feature of post-collisional extensional tectonics (southern Tuscany, Italy),, ,.
828 Tectonophysics 224, 413-423.
829 Cao, S., Neubauer, F., Bernroider, M., Genser, J., Liu, J., Friedl, G., 2017. Low-grade
830 retrogression of a high-temperature metamorphic core complex: Naxos, Cyclades,
831 Greece. Geological Society of America Bulletin 129, 93–117,
832 doi:110.1130/B31502.31501.
833 Chopra, P.N., Paterson, M.S., 1984. The role of water in the deformation of dunite. J. Geophys.
834 Res 89, 7861-7876.
835 Christofides, G., Perugini, D., Koroneos, A., Soldatos, T., Poli, G., Eleftheriadis, G., DelMoro,
836 A., Neiva, A.M., 2007. Interplay between geochemistry and magma dynamics during
837 magma interaction: an example from the Sithonia Plutonic Complex (NE Greece). Lithos
838 95, 243–266.
839 Collettini, C., Barchi, M.R., 2002. A low-angle normal fault in the Umbria region (Central
840 Italy): a mechanical model for the related microseismicity. Tectonophysics 359, 97-115.
841 Collettini, C., Barchi, M R., 2004. A comparison of structural data and seismic images for low-
842 angle normal faults in the Northern Apennines (Central Italy): constraints on activity, in:
843 Alsop, G.I., Holdsworth, R.E., McCaffrey, K.J.W., M Hands (Eds.), Flow processes in
844 faults and shear zones. Geological Society, London, pp. 95-112.
845 Collettini, C., Holdsworth, R.E., 2004. Fault zone weakening and character of slip along low-
846 angle normal faults: insights from the Zuccale fault, Elba, Italy. J. Geol. Soc. London
847 161, 1039-1051.
848 D'Agostino, N., Chamot-Rooke, N., Funiciello, R., Jolivet, L., Speranza, F., 1998. The role of
849 pre-existing thrust faults and topography on the styles of extension in the Gran Sasso
850 range (Central Italy). Tectonophysics 292, 229-254.

https://doi.org/10.5194/se-2021-11
Preprint. Discussion started: 16 February 2021

851 Daniel, J.M., Jolivet, L., 1995. Detachment faults and pluton emplacement; Elba Island
852 (Tyrrhenian Sea). Bull. Soc. géol. France 166, 341-354.
853 de Saint Blanquat, M., Horsman, M.E., Habert, G., Morgan, S., Vanderhaeghe, O., Law, R.,
854 Tikoff, B., 2011. Multiscale magmatic cyclicity, duration of pluton construction, and the
855 paradoxical relationship between tectonism and plutonism in continental arcs.
856 Tectonophysics 500, 20–33, doi:10.10 16/j.tecto.2009.2012.2009.
857 Denèle, Y., Lecomte, E., Jolivet, L., Lacombe, O., Labrousse, L., Huet, B., Le Pourhiet, L.,
858 2011. Granite intrusion in a metamorphic core complex: the example of the Mykonos
859 laccolith (Cyclades, Greece). Tectonophysics 501, 52-70,
860 doi:10.1016/j.tecto.2011.1001.1013.
861 Dini, A., Innocenti, F., Rocchi, S., Tonarini, S., Westerman, D.S., 2002. The magmatic
862 evolution of the late Miocene laccolith–pluton–dyke granitic complex of Elba Island,
863 Italy. Geol. Mag. 139, 257–279; DOI: 210.1017/S0016756802006556.
864 Duchêne, S., Aïssa, R., Vanderhaeghe, O., 2006. Pressure-Temperature-time Evolution of
865 Metamorphic Rocks from Naxos (Cyclades, Greece): constraints from Thermobarometry
866 and Rb/Sr dating Geodynamica Acta 19, 299-319.
867 Ducoux, M., Branquet, Y., Jolivet, L., Arbaret, L., Grasemann, B., Rabillard, A., Gumiaux, C.,
868 Drufin, S., 2016. Synkinematic skarns and fluid drainage along detachments: The West
869 Cycladic Detachment System on Serifos Island (Cyclades, Greece) and its related
870 mineralization. Tectonophysics 695, 1-26;
871 http://dx.doi.org/10.1016/j.tecto.2016.1012.1008.
872 Duggen, S., Hoernle, K., Van den Bogaard, P., Garbe-Schönberg, D., 2005. Post-Collisional
873 Transition from Subduction- to Intraplate-type Magmatism in the Westernmost
874 Mediterranean: Evidence for Continental-Edge Delamination of Subcontinental
875 Lithosphere.
876 Duranti, S., Palmeri, R., Pertusati, P.C., Ricci, C.A., 1992. Geological evolution and
877 metamorphic petrology of the sequences of eastern Elba (Complex II). Acta
878 Vulcanologica Marinelli Volume, 213-229.
879 Faccenna, C., Becker, T.W., 2010. Shaping mobile belts by small-scale convection. Nature 465,
880 602-605, doi:610.1038/nature09064.
881 Faccenna, C., Becker, T.W., Auer, L., Billi, A., Boschi, L., Brun, J.P., Capitanio, F.A.,
882 Funiciello, F., Horvàth, F., Jolivet, L., Piromallo, C., Royden, L., Rossetti, F., Serpelloni,
883 E., 2014. Mantle dynamics in the Mediterranean. Reviews of Geophysics 52, 283-332;
884 doi:210.1002/2013RG000444.

https://doi.org/10.5194/se-2021-11
Preprint. Discussion started: 16 February 2021

885 Farina, F., Dini, A., Innocenti, F., Rocchi, S., Westerman, D.S., 2010. Rapid incremental
886 assembly of the Monte Capanne pluton (Elba Island, Tuscany) by downward stacking of
887 magma sheets. GSA Bulletin 122, 1463–1479; doi: 1410.1130/B30112.30111.
888 Faure, M., Bonneau, M., 1988. Données nouvelles sur l'extension néogène de l'Egée: la
889 déformation ductile du granite miocène de Mykonos (Cyclades, Grèce). *C. R. Acad. Sci.*
890 *Paris* **307**, 1553-1559.
891 Faure, M., Bonneau, M., Pons, J., 1991. Ductile deformation and syntectonic granite
892 emplacement during the late Miocene extension of the Aegean (Greece). Bull. Soc. géol.
893 France 162, 3-12.
894 Fernandez, A., Barbarin, B., 1991. Relative rheology of coeval mafic and felsic magmas: nature
895 of resulting interaction processes and shape and mineral fabric of mafic microgranular
896 enclaves, in: Didier, J., Barbarin, B. (Eds.), Enclaves and Granite Petrology.Development
897 in Petrology, 13 Elsevier, pp. 263–275.
898 Fernández, C., Castro, A., 2018. Mechanical and structural consequences of magma
899 differentiation at ascent conduits: A possible origin for some mafic microgranular
900 enclaves in granites. Lithos 320–321, 49–61;
901 https://doi.org/10.1016/j.lithos.2018.1009.1004.
902 Fernandez, A., Gasquet, D., 1994. Relative rheological evolution of chemically contrasted
903 coeval magmas: example of the Tichka plutonic complex (Morocco). Contribution to
904 Mineralogy and Petrology 116, 316–326.
905 Fernandez, A., Laporte, D., 1984. Signification of low symmetry in magmatic rocks. Journal of
906 structural Geology 13, 337-347.
907 Ferrara, G., Tonarini, S., 1985. Radiometric geochronology in Tuscany : results and problems.
908 Rend. Soc. Ital. Min. Petrol. 40, 111-124.
909 Gagnevin, D., Daly, J.S., Poli, G., 2004. Petrographic, geochemical and isotopic constraints on
910 magma dynamics and mixing in the Miocene Monte Capanne monzogranite (Elba Island,
911 Italy). Lithos 78, 157–195; doi:110.1016/j.lithos.2004.1004.1043.
912 Gagnevin, D., Daly, J.S., Poli, G., 2008. Insights into granite petrogenesis from quantitative
913 assessment of the field distribution of enclaves, xenoliths and K-feldspar megacrysts in
914 the Monte Capanne pluton, Italy. Mineralogical Magazine 72, 925–940; DOI:
915 910.1180/minmag.2008.1072.1184.1925.
916 Gautier, P., Brun, J.P., 1994a. Crustal-scale geometry and kinematics of late-orogenic extension
917 in the central Aegean (Cyclades and Evvia island). Tectonophysics 238, 399-424;
918 doi:310.1016/0040-1951(1094)90066-90063.

https://doi.org/10.5194/se-2021-11
Preprint. Discussion started: 16 February 2021

919 Gautier, P., Brun, J.P., 1994b. Ductile crust exhumation and extensional detachments in the
920 central Aegean (Cyclades and Evvia islands). Geodinamica Acta 7, 57-85.
921 Gautier, P., Brun, J.P., Jolivet, L., 1993. Structure and kinematics of upper Cenozoic
922 extensional detachement on Naxos and Paros (Cyclades Islands, Greece). Tectonics 12,
923 1180-1194; doi:1110.1029/1193TC01131.
924 Gerya, T., Yuen, D., 2003. Rayleigh-Taylor instabilities from hydration and melting propel
925 'cold plumes' at subduction zones. Earth Planet. Sci. Lett. 212, 47-62.
926 Grasemann, B., Petrakakis, K., 2007. Evolution of the Serifos Metamorphic Core Complex.
927 Journal of the Virtual Explorer 27, 1-18.
928 Hansen, F.D., Carter, N.L., 1982. Creep of selected crustal rocks at 1000 MPa. Trans. Am.
929 Geophys. Union 63, 437.
930 Hirschmann, M.M., 2000. Mantle solidus: experimental constraints and the effects of peridotite
931 composition. Geochem. Geophys. Geosyst 1, 2000GC000070.
932 Huet, B., Labrousse, L., Jolivet, L., 2009. Thrust or detachment? Exhumation processes in the
933 Aegean: insight from a field study on Ios (Cyclades, Greece). Tectonics 28, TC3007,
934 doi:3010.1029/2008TC002397.
935 Huet, B., Le Pourhiet, L., Labrousse, L., Burov, E., Jolivet, L., 2011. Post-orogenic extension
936 and metamorphic core complexes in a heterogeneous crust: the role of crustal layering
937 inherited from collision. Application to the Cyclades (Aegean domain). Geophysical J.
938 Int. 184, 611–625, doi: 610.1111/j.1365-1246X.2010.04849.x.
939 Huet, B., Le Pourhiet, L., Labrousse, L., Burov, E., Jolivet, L., 2011. Formation of metamorphic
940 core complex in inherited wedges: a thermomechanical modelling study. Earth Planet.
941 Sci. lett. doi:10.1016/j.epsl.2011.07.004.
942 Innocenti, F., Westerman, D.S., Rocchi, S., Tonarini, S., 1997. The Montecristo monzogranite
943 (Northern Tyrrhenian Sea, Italy): a collisional pluton in an extensional setting. Geological
944 Journal 32, 131-151.
945 Jansen, J.B.H., 1977. Metamorphism on Naxos, Greece. Utrecht University.
946 Jolivet, L., Augier, R., Faccenna, C., Negro, F., Rimmele, G., Agard, P., Robin, C., Rossetti,
947 F., Crespo-Blanc, A., 2008. Subduction, convergence and the mode of backarc extension
948 in the Mediterranean region. Bull Soc géol France 179, 525-550.
949 Jolivet, L., Brun, J.P., 2010. Cenozoic geodynamic evolution of the Aegean region. Int. J. Earth
950 Science 99, 109–138, DOI: 110.1007/s00531-00008-00366-00534.
951 Jolivet, L., Faccenna, C., 2000. Mediterranean extension and the Africa-Eurasia collision.
952 Tectonics 19, 1095-1106; doi:1010.1029/2000TC900018.

https://doi.org/10.5194/se-2021-11
Preprint. Discussion started: 16 February 2021

953 Jolivet, L., Faccenna, C., Goffé, B., Mattei, M., Rossetti, F., Brunet, C., Storti, F., Funiciello,
954 R., Cadet, J.P., Parra, T., 1998. Mid-crustal shear zones in post-orogenic extension: the
955 northern Tyrrhenian Sea case. J. Geophys. Res. 103, 12123-12160; doi:12110.11029/
956 12197JB03616.
957 Jolivet, L., Lecomte, E., Huet, B., Denèle, Y., Lacombe, O., Labrousse, L., Le Pourhiet, L.,
958 Mehl, C., 2010. The North Cycladic Detachment System. Earth and Planet. Sci. Lett. 289
959 87-104, doi:110.1016/j.epsl.2009.1010.1032.
960 Jolivet, L., Menant, A., Sternai, P., Rabillard, A., Arbaret, L., Augier, R., Laurent, V.,
961 Beaudoin, A., Grasemann, B., Huet, B., Labrousse, L., Le Pourhiet, L., 2015. The
962 geological signature of a slab tear below the Aegean. Tectonophysics 659 166–182, 166–
963 182, doi:110.1016/j.tecto.2015.1008.1004.
964 Jolivet, L., Sautter, V., Moretti, I., Vettor, T., Papadopoulou, Z., Augier, R., Denèle, Y.,
965 Arbaret, L., 2021. Anatomy and evolution of a migmatite-cored extensional metamorphic
966 dome and interaction with syn-kinematic intrusions, the Mykonos-Delos-Rheneia MCC.
967 Journal of Geodynamics, accepted.
968 Juteau, M., Michard, A., Zimmermann, J.L., Albarede, F., 1984. Isotopic heterogeneities in the
969 granitic intrusion of Monte Capanne (Elba island, Italy) and dating concepts. Journal of
970 Petrology 25, 532-545.
971 Katzir, Y., Matthews, A., Garfunkel, Z., Schliestedt, M., Avigad, D., 1996. The tectono-
972 metamorphic evolution of a dismembered ophiolite (Tinos, Cyclades, Greece). Geol.
973 Mag. 133, 237-254.
974 Keay, S., Lister, G., Buick, I., 2001. The timing of partial melting, Barrovian metamorphism
975 and granite intrusion in the Naxos metamorphic core complex, Cyclades, Aegean Sea,
976 Greece. Tectonophysics 342, 275-312; doi:210. 1016/S0040-1951(1001)00168-00168.
977 Keller, J.V., Pialli, G., 1990. Tectonics of the island of Elba: a reappraisal. Boll. Soc. Geol. It.
978 109, 413-425.
979 Keller, J.V.A., Minelli, G., Pialli, G., 1994. Anatomy of late orogenic extension: the Northern
980 Apennines case. Tectonophysics 238, 275-294.
981 Kruckenberg, S.C., Vanderhaeghe, O., Ferré, E.C., Teyssier, C., Whitney, D.L., 2011. Flow of
982 partially molten crust and the internal dynamics of a migmatite dome, Naxos, Greece:
983 internal dynamics of the Naxos dome. Tectonics 30, 1–24, doi:10.1029/2010TC002751.
984 Kuhlemann, J., Frisch, W., Dunkl, I., Kázmér, M., Schmiedl, G., 2004. Miocene siliciclastic
985 deposits of Naxos Island: Geodynamic and environmental implications for the evolution
986 of the southern Aegean Sea (Greece), in: Bernet, M., Spiegel, C. (Eds.), Detrital

thermochronology - Provenance analysis, exhumation, and landscape evolution of mountain belts:. Geological Society of America, pp. 51-65.

Labrousse, L., Huet, B., Le Pourhiet, L., Jolivet, L., Burov, E., 2016. Rheological implications of extensional detachments: Mediterranean and numerical insights. Earth-Science Reviews 161, 233-258; http://dx.doi.org/210.1016/j.earscirev.2016.1009.1003.

Lamont, T.N., Roberts, N.M.W., Searle, M.P., Gopon, P., Waters, D.J., Millar, I., 2020. The age, origin, and emplacement of the Tsiknias Ophiolite, Tinos, Greece. Tectonics 39, e2019TC00567; https://doi.org/ 00510.01029/02019TC005677.

Laurent, V., Beaudoin, A., Jolivet, L., Arbaret, L., Augier, R., Rabillard, A., 2015. Interrelations between extensional shear zones and synkinematic intrusions: The example of Ikaria Island (NE Cyclades, Greece). Tectonophysics 651-652, 152-171, http://dx.doi.org/110.1016/j.tecto.2015.1003.1020.

Lee, J., Lister, G.S., 1992. Late Miocene ductile extension and detachment faulting, Mykonos, Greece. Geology 20, 121-124; doi:110.1130/0091-7613(1992)1020<0121:LMDEAD>1132.1133.CO;1132.

Le Pourhiet, L., Burov, E., Moretti, I., 2004. Rifting through a stack of inhomogeneous thrusts (the dipping pie concept). Tectonics 23, doi:10.1029/2003TC001584.

Lecomte, E., Le Pourhiet, L., Lacombe, O., 2012. Mechanical basis for the activity of low angle normal faults. Geophysical Res. Lett. 39, L03307; doi:03310.01029/02011GL050756.

Lecomte, E., Le Pourhiet, L., Lacombe, O., Jolivet, L., 2011. A continuum mechanics approach to quantify brittle strain on weak faults: application to the extensional reactivation of shallow-dipping discontinuities. Geophys. J. Int. 184, 1-11, doi: 10.1111/j.1365-1246X.2010.04821.x.

Liotta, D., Brogi, A., Meccheri, M., Dini, A., Bianco, C., Ruggieri, G., 2015. Coexistence of low-angle normal and high-angle strike- to oblique-slip faults during Late Miocene mineralization in eastern Elba Island (Italy). Tectonophysics 660, , 17-34; http://dx.doi.org/10.1016/j.tecto.2015.1006.1025.

Lister, G.S., Baldwin, S., 1993. Plutonism and the origin of metamorphic core complexes. Geology 21, 607-610; doi:610.1130/0091-7613(1993)1021<0607:PATOOM>1132.1133.CO;1132.

Lister, G.S., Snoke, A.W., 1984. S-C mylonites. Journal of Structural Geology 6, 617-638.

Maineri, C., Benvenuti, M., Costagliola, P., Dini, A., Lattanzi, P., Ruggieri, G., Villa, I.M., 2003. Sericitic alteration at the La Crocetta deposit (Elba Island, Italy): interplay between

https://doi.org/10.5194/se-2021-11
Preprint. Discussion started: 16 February 2021

magmatism, tectonics and hydrothermal activity. Mineralium Deposita 38, 67–86; DOI 10.1007/s00126-00002-00279-00122.

Martha, S.O., Dörr, W., Gerdes, A., Petschick, R., Schastok, J., Xypolias, P., Zulauf, G., 2016. New structural and U–Pb zircon data from Anafi crystalline basement (Cyclades, Greece): constraints on the evolution of a Late Cretaceous magmatic arc in the Internal Hellenides. International Journal of Earth Sciences 105, 2031–2060, doi:2010.1007/s00531-00016-01346-00538.

Menant, A., Jolivet, L., Augier, R., Skarpelis, N., 2013. The North Cycladic Detachment System and associated mineralization, Mykonos, Greece: insights on the evolution of the Aegean domain. Tectonics 32, 433–452, doi:410.1002/tect.20037.

Miller, C.F., McDowell, S.M., Mapes, R.W., 2003. Hot and cold granites? Implications of zircon saturation temperatures and preservation of inheritance. Geology 31, 529-532.

Musumeci, G., Vaselli, L., 2012. Neogene deformation and granite emplacement in the metamorphic units of northern Apennines (Italy): Insights from mylonitic marbles in the Porto Azzurro pluton contact aureole (Elba Island). Geosphere 8, 470–490; doi:410.1130/GES00665.00661.

Pandeli, E., Giusti, R., Elter, F.M., Orlando, A., Orti, L., 2018. Structural setting and metamorphic evolution of a contact aureole: the example of the Mt. Capanne pluton (Elba Island, Tuscany, italy). Ofioliti 43, 41-73; doi: 10.4454/ofioliti.v4443i4451.4455.

Paterson, S.R., 2009. Magmatic tubes, pipes, troughs, diapirs, and plumes: Late-stage convective instabilities resulting in compositional diversity and permeable networks in crystal-rich magmas of the Tuolumne batholith, Sierra Nevada, California. Geosphere 5, 496–527; doi: 410.1130/GES00214.00211.

Pauselli, C., Ranalli, G., 2017. Effects of lateral variations of crustal rheology on the occurrence of post- orogenic normal faults: The Alto Tiberina Fault (Northern Apennines, Central Italy). Tectonophysics 721, 45-55; http://dx.doi.org/10.1016/j.tecto.2017.1009.1008.

Pe-Piper, G., 2000. Origin of S-type granites coeval with I-type granites in the Hellenic subduction system, Miocene of Naxos, Greece. European Journal of Mineralogy 12, 859–875, doi:810.1127/ejm/1112/1124/0859.

Pe-Piper, G., Kotopouli, C.N., Piper, D.J.W., 1997. Granitoid rocks of Naxos, Greece: regional geology and petrology. Geological Journal 32, 153–171, doi:110.1002/(SICI)1099-1034(199706)199732: 199702<199153::AID-GJ199737>199703.199700.CO;199702-199701.

https://doi.org/10.5194/se-2021-11
Preprint. Discussion started: 16 February 2021

1053 Pe-Piper, G., Piper, D.J.W., 2002. The igneous rocks of Greece. The anatomy of an orogen.
1054 Gebrüder Borntraeger, Berlin-Stuttgart.
1055 Pe-Piper, G., Piper, D.J.W., 2007. Neogene back-arc volcanism of the Aegean: new insights
1056 into the relationship between magmatism and tectonics, in: Beccaluva, L., Bianchini, G.
1057 (Eds.), Cenozoic Volcanism in the Mediterranean Area. Geological Society of America,
1058 pp. 17–31, doi: 10.1130/2007.2418(1102).
1059 Pe-Piper, G., Piper, D.J.W., Matarangas, D., 2002. Regional implications of geochemistry and
1060 style of emplacement of Miocene I-type diorite and granite, Delos, Cyclades, Greece.
1061 Lithos 60, 47–66, doi:10.1016/S0024-4937(1001)00068-00068.
1062 Perrin, M., 1975. L'ile d'Elbe et la limite Alpes-Apennins: données sur la structure géologique
1063 et l'évolution tectogénétique de l'Elbe alpine et de l'Elbe apennine. Bull. Soc. Geol. It. 94,
1064 1929-1955.
1065 Pertusati, P.C., Raggi, G., Ricci, C.A., Duranti, S., Palmeri, R., 1993. Evoluzione post-
1066 collisionale dell'Elba centro-orientale. Mem. Soc. Geol. It. 49, 297-312.
1067 Perugini, D., Poli, G., Rocchi, S., 2005. Development of viscous fingering between mafic and
1068 felsic magmas: evidence from the Terra Nova Intrusive Complex (Antarctica).
1069 Mineralogy and Petrology 83, 151–166.
1070 Petrakakis, K., Iglseder, C., Zámolyi, A., Rambousek, C., Grasemann, B., Draganitis, E., Kurka,
1071 A., Photiades, A., 2010. Serifos Island, Geological Map of Greece. Institute of Geology
1072 and Mineral Exploration (IGME).
1073 Poli, G., Manetti, P., Tommasini, S., 1989. A petrological review on Miocene–Pliocene
1074 intrusive rocks from Southern Tuscany and Tyrrhenian Sea (Italy). Periodico di
1075 Mineralogia 58, 109 – 126.
1076 Poli, G.E., Tommasini, S., 1991. Model for the Origin and Significance of Microgranular
1077 Enclaves in Calc-alkaline Granitoids. Journal of Petrology 32, 657-666.
1078 Rabillard, A., Arbaret, L., Jolivet, L., Le Breton, N., Gumiaux, C., Augier, R., Grasemann, B.,
1079 2015. Interactions between plutonism and detachments during Metamorphic Core
1080 Complex formation, Serifos Island (Cyclades, Greece). Tectonics 34, 1080-1106, DOI:
1081 1010.1002/2014TC003650.
1082 Rabillard, A., Jolivet, L., Arbaret, L., Bessière, E., Laurent, V., Menant, A., Augier, R.,
1083 Beaudoin, A., 2018. Synextensional Granitoids and Detachment Systems Within
1084 Cycladic Metamorphic Core Complexes (Aegean Sea, Greece): Toward a Regional
1085 Tectonomagmatic Model. Tectonics 37; https://doi.org/10.1029/2017TC004697.

https://doi.org/10.5194/se-2021-11
Preprint. Discussion started: 16 February 2021

1086 Ranalli, G., Murphy, D.C., 1987. Rheological stratification of the lithosphere. Tectonophysics
1087 132, 281-295.
1088 Reinecke, T., Altherr, R., Hartung, B., Hatzipanagiotou, K., Kreuzer, H., Harre, W., Klein, H.,
1089 Keller, J., Geenen, E., Böger, H., 1982. Remnants of a late Cretaceous high temperature
1090 bet on the island of Anafi (Cyclades, Greece). N. Jb. Miner. Abh 145, 157-182.
1091 Rey, P.F., Teyssier, C., Whitney, D.L., 2009. The Role of Partial Melting and Extensional
1092 Strain Rates in the Development of Metamorphic Core Complexes. Tectonophysics 477,
1093 135-144, doi: 110.1016/j.tecto.2009.1003.1010.
1094 Ring, U., 2007. The geology of Ikaria Island: The Messaria extensional shear zone, granites
1095 and the exotic Ikaria nappe. Journal of the Virtual Explorer 27, 1–32.
1096 Ring, U., Glodny, J., Will, T., Thomson, S., 2010. The Hellenic Subduction System: High-
1097 Pressure Metamorphism, Exhumation, Normal Faulting, and Large-Scale Extension.
1098 Annu. Rev. Earth Planet. Sci. 38, 45–76, 10.1146/annurev.earth.050708.170910.
1099 Rocchi, S., Westerman, D.S., Dini, A., Innocenti, F., Tonarini, S., 2002. Two-stage growth of
1100 laccoliths at Elba Island, Italy. Geology 30, 983–986.
1101 Roche, V., Sternai, P., Guillou-Frottier, L., Menant, A., Jolivet, L., Bouchot, V., Gerya, T.,
1102 2018. Emplacement of metamorphic core complexes and associated geothermal systems
1103 controlled by slab dynamics. Earth and Planetary Science Letters 498 322–333;
1104 https://doi.org/310.1016/j.epsl.2018.1006.1043.
1105 Rochira, F., Caggianelli, A., de Lorenzo, S., 2018. Regional thermo-rheological field related to
1106 granite emplacement in the upper crust: implications for the Larderello area (Tuscany,
1107 Italy). Geodinamica Acta 30, 225-240, DOI: 210.1080/09853111.09852018.01488912.
1108 Rodríguez, C., Castro, A., 2019. Origins of mafic microgranular enclaves and enclave swarms
1109 in granites: Field and geochemical relations. GSA Bulletin 131, 635–660;
1110 https://doi.org/610.1130/B32028.32021.
1111 Rosenberg, C.L., Handy, M.R., 2005. Experimental deformation of partially melted granite
1112 revisited: implications for the continental crust. Journal of metamorphic Geology 23
1113 Rossetti, F., Balsamo, F., Villa, I.M., Bouybaouenne, M., Faccenna, C., Funiciello, R., 2008.
1114 Pliocene-Pleistocene HT-LP metamorphism during multiple granitic intrusions in the
1115 southern branch of the Larderello geothermal field (southern Tuscany, Italy). J. Geol.
1116 Soc. London 165, 247-262.
1117 Rossetti, F., Faccenna, C., Jolivet, L., Funiciello, R., Goffé, B., Tecce, F., Brunet, C., Monié,
1118 P., Vidal, O., 1999. Structural signature and exhumation P-T-t path of the Gorgona
1119 blueschist sequence (Tuscan Archipelago, Italy). Ofioliti 26, 175-186.

https://doi.org/10.5194/se-2021-11
Preprint. Discussion started: 16 February 2021

1120 Rossetti, F., Faccenna, C., Jolivet, L., Tecce, F., Funiciello, R., Brunet, C., 1999b. Syn- versus
1121 post-orogenic extension in the Tyrrhenian Sea, the case study of Giglio Island (Northern
1122 Tyrrhenian Sea, Italy). Tectonophysics 304, 71-93; doi:10.1016/S0040-
1123 1951(1098)00304-00307.
1124 Rossetti, F., Tecce, F., 2008. Composition and evolution of fluids during skarn development in
1125 the Monte Capanne thermal aureole, Elba Island, central Italy. Geofluids 8 167–180; doi:
1126 110.1111/j.1468-8123.2008.00215.x.
1127 Rossetti, F., Tecce, F., Billi, A., Brilli, M., 2007. Patterns of fluid flow in the contact aureole
1128 of the Late Miocene Monte Capanne pluton (Elba Island, Italy): the role of structures and
1129 rheology. Contrib Mineral Petrol 53, 743–760; DOI 710.1007/s00410-00006-00175-
1130 00413.
1131 Salemink, J., 1985. Skarn and ore formation at Serifos, Greece, as a consequence of
1132 granodiorite intrusion. University of Utrecht, Netherlands.
1133 Sanchez-Gomez, M., Avigad, D., Heiman, A., 2002. Geochronology of clasts in allochthonous
1134 Miocene sedimentary sequences on Mykonos and Paros islands: implications for back-
1135 arc extension in the Aegean Sea. J. Geol. Soc. London 159, 45-60; doi:10.1144/0016-
1136 764901031.
1137 Saupé, F., Marignac, C., Moine, B., Sonet, J., Zimmermann, J.L., 1982. Datation par les
1138 méthodes K/Ar et Rb/Sr de quelques roches de la partie orientale de l'ile d'Elbe (Province
1139 de Livourne, Italie). Bulletin de Minéralogie 105, 236-245.
1140 Savelli, C., 1988. Late Oligocene to Recent episodes of magmatism in and around the
1141 Tyrrhenian Sea: implication for the process of opening in a young inter-arc basin of intra-
1142 orogenic (Mediterranean) type. Tectonophysics 146, 163-181.
1143 Savelli, C., 2002a. Tectono-magmatic lineaments and subduction in the central Mediterranean
1144 and southern Italy during the past 8 Ma. Boll. Soc. Geol. It., 121, 231-242.
1145 Savelli, C., 2002b. Time–space distribution of magmatic activity in the western Mediterranean
1146 and peripheral orogens during the past 30 Ma (a stimulus to geodynamic considerations).
1147 Journal of Geodynamics 34, 99–126.
1148 Savelli, C., 2015. Fast Episodes of West- Mediterranean-Tyrrhenian Oceanic Opening and
1149 Revisited Relations with Tectonic Setting. Scientific Reports 5:, 14271; DOi:
1150 14210.11038/srep14271.
1151 Scheffer, C., Vanderhaeghe, O., Lanari, P., Tarantola, A., Ponthus, L., Photiades, A., France,
1152 L., 2016. Syn- to post-orogenic exhumation of metamorphic nappes: Structure and

https://doi.org/10.5194/se-2021-11
Preprint. Discussion started: 16 February 2021

thermobarometry of the western Attic-Cycladic metamorphic complex (Lavrion, Greece). Journal of Geodynamics 96, 174–193; http://dx.doi.org/110.1016/j.jog.2015.1008.1005.

Schubert, M., Driesner, T., Gerya, T.V., Ulmer, P., 2013. Mafic injection as a trigger for felsic magmatism: A numerical study. Geochem. Geophys. Geosyst. 14, 1910–1928, doi:1910.1002/ggge.20124.

Serri, G., Innocenti, F., Manetti, P., 1993. Geochemical and petrological evidence of the subduction of delaminated Adriatic continental lithosphere in the genesis of the Neogene-Quaternary magmatism of central Italy. Tectonophysics 223, 117-147.

Seward, D., Vanderhaeghe, O., Siebenaller, L., Thomson, S., Hibsch, C., Zingg, A., Holzner, P., Ring, U., Duchêne, S., 2009. Cenozoic tectonic evolution of Naxos Island through a multi-faceted approach of fission-track analysis, in: Ring, U., Wernicke, B. (Eds.), Extending a continent: architecture, rheology and heat budget. Geological Society, London, pp. 179-196; doi:110.1144/SP1321.1149.

Soukis, K.I., Papanikolaou, D.J., 2004. Contrasting geometry between Alpine and Late-to-post-Alpine tectonic structures in Anafi Island (Cyclades). Bulletin of the Geological Society of Greece vol. 2004 XXXVI, 1688-1696.

Spakman, W., Wortel, R., 2004. A tomographic view on Western Mediterranean geodynamics, in: Cavazza, W., Roure, F.M., Spakman, W., Stampfli, G.M., Ziegler, P.A. (Eds.), The TRANSMED Atlas - The Mediterranean region from crust to Mantle. Springer, Berlin, Heidelberg, pp. 31-52.

St. Seymour, K., Zouzias, D., Tombros, S., Kolaiti, E., 2009. Geochemistry of the Serifos pluton (Cycladic islands) and associated iron oxide and sulfide ores: Skarn or metamorphosed exhalite deposits? Neues Jahrbuch für Mineralogie - Abhandlungen 186, 249-270; doi:210.1127/0077-7757/2009/0143.

Thompson, A.B., Connolly, J.A.D., 1995. Melting of the continental crust: some thermal and petrological constraints on anatexis in continental collision zones and other tectonic settings. J. Geoph. Res. 100, 15565-15579.

Tirel, C., Brun, J.P., Burov, E., 2004. Thermo-mechanical modeling of extensional gneiss domes, in: Whitney, D.L., Teyssier, C., Siddoway, C.S. (Eds.), Gneiss domes in orogeny, Boulder, Colorado, pp. 67-78.

Tirel, C., Brun, J.P., Burov, E., 2008. Dynamics and structural development of metamorphic core complexes. J. Geoph. Res. 113, doi:10.1029/2005JB003694.

Tombros, S.F., St. Seymour, K., Williams-Jones, A.E., Zhai, D., Liu, J., 2015. Origin of a barite-sulfide ore deposit in the Mykonos intrusion, cyclades: Trace element, isotopic,

https://doi.org/10.5194/se-2021-11
Preprint. Discussion started: 16 February 2021

1187 fluid inclusion and raman spectroscopy evidence. Ore Geology Reviews 67, 139–157;
1188 http://dx.doi.org/110.1016/j.oregeorev.2014.1011.1016.
1189 Trevisan, L., 1950. L'Elba orientale e la sua tettonica scivolamento par gravità. Mem. Instit.
1190 Geol. It. Pavia 70, 435-470.
1191 Urai, J.L., Shuiling, R.D., Jansen, J.B.H., 1990. Alpine deformation on Naxos (Greece), in:
1192 Knipe, R.J., Rutter, E.H. (Eds.), Deformation mechanisms, Rheology and tectonics. *Geol.*
1193 *Soc. spec. Pub.*, pp. 509-522; doi:510.1144/GSL.SP.1990.1054.1101.1147.
1194 van der Laan, S.R., Wyllie, P.J., 1993. Experimental Interaction of Granitic and Basaltic
1195 Magmas and Implications for Mafic Enclaves. Journal of Petrology 34, 491-517.
1196 Vanderhaeghe, O., 2004. Structural development of the Naxos migmatite dome, in: Whitney,
1197 D.L., Teyssier, C., Siddoway, C.S. (Eds.), Gneiss domes in orogeny. Geological Society
1198 of America, Boulder, Colorado, pp. 211-227.
1199 Vanderhaeghe, O., 2009. Migmatites, granites and orogeny: Flow modes of partially-molten
1200 rocks and magmas associated with melt/solid segregation in orogenic belts.
1201 Tectonophysics 477, 119–134, doi:110. 1016/j.tecto.2009.1006.1021.
1202 Vanderhaeghe, O., Kruckenberg, S.C., Gerbault, M., Martin, L., Duchêne, S., Deloule, S., 2018.
1203 Crustal-scale convection and diapiric upwelling of a partially molten T orogenic root
1204 (Naxos dome, Greece). Tectonophysics 746; https://doi.org/10.1016/j.tecto.2018.03.007,
1205 459–469
1206 Vernon, R.H., 1986. K-feldspar megacrysts in granites - phenocrysts, not porphyroblasts. Earth-
1207 Sci. Rev. 23, 1-63.
1208 Vernon, R.H., Paterson, S.R., 2008. How late are K-feldspar megacrysts in granites? Lithos
1209 104, 327–336; doi:310.1016/j.lithos.2008.1001.1001.
1210 Weinberg, R.F., Hasalová, P., 2015. Water-fluxed melting of the continental crust: A review.
1211 Lithos 212–215, 158–188; http://dx.doi.org/110.1016/j.lithos.2014.1008.1021.
1212 Weinberg, R.F., Sial, A.N., Pessoa, R.R., 2001. Magma flow within the Tavares pluton,
1213 Northeastern Brazil: compositional and thermal convection. Bull. Geol. Soc. Am. 113,
1214 508–520.
1215 Westerman, D.S., Dini, A., Innocenti, F., Rocchi, S., 2004. Rise and fall of a nested Christmas-
1216 tree laccolith complex, Elba Island, Italy, in: Breitkreuz, C., Petford, N. (Eds.), Physical
1217 geology of high level magmatic systems. Geological Society, London, pp. 195-213.
1218 Westerman, D.S., Innocenti, F., Tonarini, S., Ferrara, G., 1993. The Pliocene intrusions of the
1219 island of Giglio. Mem. Soc. Geol. It. 49, 345-363.

https://doi.org/10.5194/se-2021-11
Preprint. Discussion started: 16 February 2021

1220 Wiebe, R.A., Jellinek, A.M., Hodge, K.F., 2017. New insights into the origin of ladder dikes:
1221 Implications for punctuated growth and crystal accumulation in the Cathedral Peak
1222 granodiorite. Lithos 277, 241–258; http://dx.doi.org/210.1016/j.lithos.2016.1009.1015.
1223 Wortel, M.J.R., Spakman, W., 2000. Subduction and slab detachment in the Mediterranean-
1224 Carpathian region. Science 290, 1910-1917.
1225
1226

https://doi.org/10.5194/se-2021-11
Preprint. Discussion started: 16 February 2021

Appendix A Table A1

		Sediments (2)	*Upper crust (1)*	*Middle crust(2)*	*Lower crust(1)*	*Lithospheric mantle(3)*	*Asthenospheric mantle(3)*
Density(kg.m^{-3})	ρ_r	2400	2700	2700	2700	3300	3300
Pre exp. Factor (MPa^{-n}s^{-1})	A	2.4	3.3	2.4	3.3	3.5	3.5
Activation energy(kJ)	Q	156	186	156	219	532	532
Stress exponent	n	6.7 10^{-6}	2 10^{-6}	6.7 10^{-6}	1.3 10^{-3}	2.5 10^{4}	2.5 10^{4}
Melt density(kg.m^{-3})	ρ_m	-	2400	2400	2400	2800	2800
Melt viscosity	η_m	-	10^{17}	10^{17}	10^{17}	10^{12}	10^{12}
Heat production (Wm^{-3})	H	1.67 10^{-10}	1.67 10^{-10}	0	0	0	0
Thermal diffusivity	κ	10^{-6}	10^{-6}	10^{-6}	10^{-6}	10^{-6}	5 10^{-6}

Table A1 : Values and notation for variable physical parameters. Parameters for dislocation creep come from 1 (Ranalli and Murphy, 1987), 2 (Hansen and Carter, 1982) and 3 (Chopra and Paterson, 1984). Other constant parameters include: friction ϕ and cohesion C which varies linearly with plastic strain in range [0,1] respectively from 30° to 20° and from 20 MPas to 2 MPa; Coefficient of thermal expansion and compressibility that are set to 3.10^{-5}K^{-1} and 10^{-11} Pa^{-1}.

https://doi.org/10.5194/se-2021-11
Preprint. Discussion started: 16 February 2021

1237 # Appendix A, figure A1 and A2:

1238

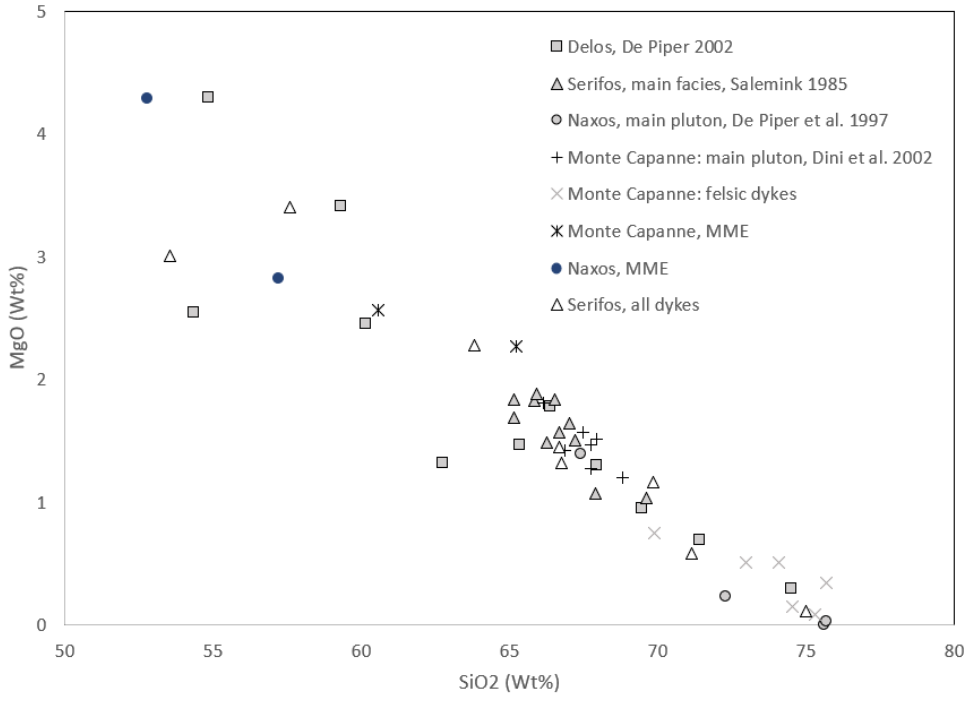

1239

1240

1241 *Figure A1: MgO v. Si02 Harker diagram showing the negative correlation between whole rock*
1242 *MgO and SiO2 content for three, I-type hornblende-biotite bearing, representative*
1243 *Aegean granites. Data from Delos intrusion (Pe-Piper et al., 2002), Serifos (Salemink,*
1244 *1985) and Naxos (Pe-Piper et al., 1997). Mixing/mingling processes between mafic*
1245 *mantle-derived melts and acid magmas produce composite batholiths (Poli and*
1246 *Tommasini, 1990) as illustrated by the case of the Elba Island magmatic complex showed*
1247 *for comparison (See Dini et al. 2002 for explanation). MME = Mafic Microgranular*
1248 *Enclaves.*

1249

https://doi.org/10.5194/se-2021-11
Preprint. Discussion started: 16 February 2021

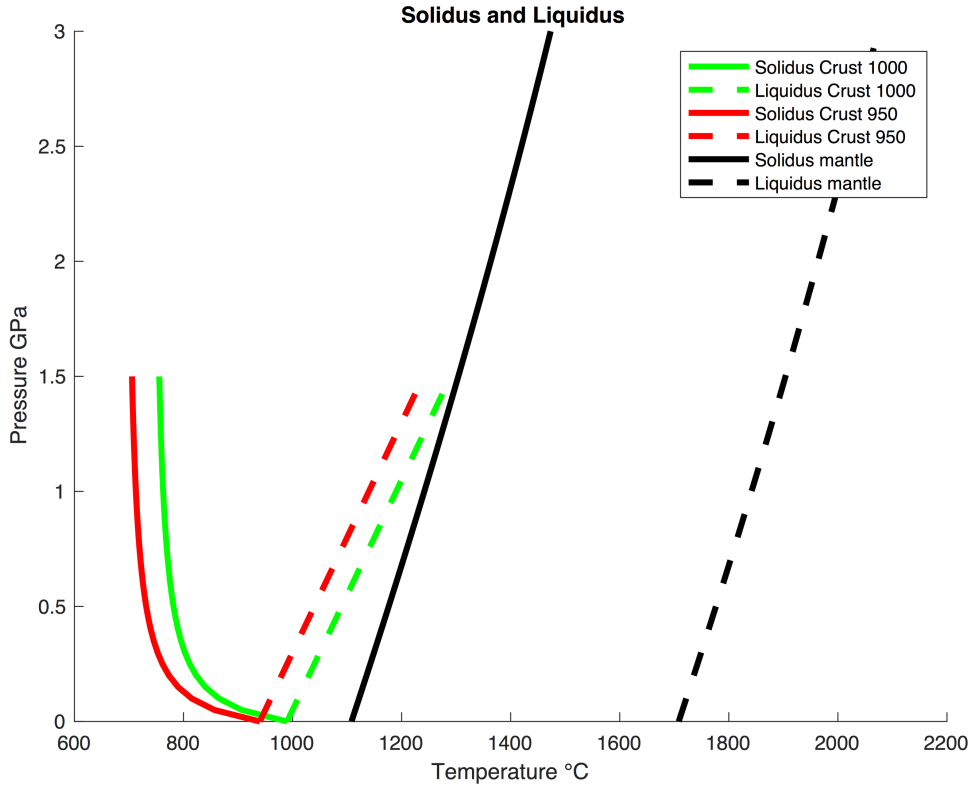

Figure A2: Solidus and liquidus as a function of pressure and temperature for mantle and crust (950 and 1000°C).